Uncertain reduced-order modeling for unsteady aerodynamics with interval parameters and its application on robust flutter boundary prediction

Xianjia Chen [a], Zhiping Qiu [a,*], Xiaojun Wang [a], Yunlong Li [b], Ruixing Wang [c]

[a] *Institute of Solid Mechanics, Beihang University, Beijing 100191, China*
[b] *Department of Mechanical Science and Engineering, University of Illinois at Urbana-Champaign, Urbana, IL 61801, United States*
[c] *Key Laboratory for Mechanics in Fluid Solid Coupling Systems, Institute of Mechanics, Chinese Academy of Sciences, Beijing 100190, China*

ARTICLE INFO

ABSTRACT

Computational fluid dynamics based unsteady aerodynamic reduced-order models can significantly improve the efficiency of transonic aeroelastic analysis. In this paper, the concept of the conventional model reduction method based on the system identification theory is extended to aerodynamic subsystems with the consideration of computational fluid dynamics-induced interval uncertainties in simulation to get the aerodynamic reduced-order model as uncertain as the original aerodynamic subsystem. The interval estimation of identified coefficients involved in the uncertain reduced-order model is obtained by utilizing the first-order interval perturbation method. The stability problem of the interval aeroelastic state-space model formulated based on the constructed uncertain aerodynamic reduced-order model is equivalently transformed into a standard interval eigenvalue problem associated with a real non-symmetric interval matrix in which the interval bounds of eigenvalues are evaluated by virtue of the first-order interval matrix perturbation algorithm. A new stability criterion for the interval aeroelastic state matrix is defined to predict the robust flutter boundary of the concerned uncertain aeroelastic system. Two numerical examples with respect to the uncertain aerodynamic ROM constructions and robust flutter boundary predictions of the two-dimensional Isogai wing and the three-dimensional AGARD 445.6 wing in transonic regime are implemented to assess the validity and accuracy of the presented approach. The obtained results are also compared with Monte Carlo simulation solutions as well as numerical and experimental results in the literatures indicating that the proposed method can provide a more robust and conservative prediction on the flutter boundary of an aeroelastic system compared with conventional deterministic aeroelastic analysis approaches.

© 2017 Elsevier Masson SAS. All rights reserved.

1. Introduction

Classical aeroelasticity is the study dealing with the stability and response of elastic structures under the interaction of inertial forces, structural, and aerodynamic. Fluid–structure interaction effects are of paramount importance regarding the limits of the flight envelope and therefore strongly influence safety and efficiency requirements [1].

The issue of dynamic stability, which is commonly referred to as the flutter analysis, is an important branch in the field of aeroelasticity. The accurate prediction of unsteady aerodynamic forces is an essential foundation for flutter analysis. Due to the inherent superiority over the traditional linear potential flow theory for ad-

dressing distinct aerodynamic nonlinearities in the transonic flight regime or at a high angle of attack, the computational fluid dynamics (CFD) techniques have been widely used in aerodynamic calculations during the last several decades. However, in terms of efficiency, the high-fidelity CFD approach requires expensive computational costs associated with the meticulous descriptions of flow in both spatial and temporal dimensions, which limits its further applications in aeroelastic analysis, optimal design and control.

To alleviate the contradiction between the computational efficiency and predictive accuracy, increasing attention has been paid to the CFD-based reduced-order models (ROMs), which provide an alternate way to effectively model unsteady aerodynamic loads. The CFD-based ROM seeks to construct a simple mathematical representation model, which can capture the dominant behavior of the aerodynamic or aeroelastic system and can be convenient to

Nomenclature

a	dimensionless distance of elastic axis behind midchord
$\mathbf{A}_{as}^{I}$	interval state matrix of uncertain aeroelastic model
$\mathbf{A}_i$	coefficient matrices of $\mathbf{f}(k-i)$
b	airfoil semichord
$\mathbf{B}_j$	coefficient matrices of $\boldsymbol{\xi}(k-j)$
$\mathbf{e}$	output error vector
E	Young's modulus
$\mathbf{f}$	system output (generalized aerodynamic coefficient) vector
$\mathbf{F}$	generalized aerodynamic force vector
G	shear modulus
$\mathbf{G}$	generalized structural damping matrix
h	plunge displacement of elastic axis
$J(\boldsymbol{\theta})$	criterion function with respect to $\boldsymbol{\theta}$
k	discrete time step
$\mathbf{K}$	generalized structural stiffness matrix
K_h	plunge spring constant
K_α	pitch spring constant
L	data length of system input and output
M	modal truncation order of structural subsystem
$\mathbf{M}$	generalized structural mass matrix
Ma	Mach number of freestream
na	output delay orders of aerodynamic model
nb	input delay orders of aerodynamic model
q	freestream dynamic pressure
q^*	critical dynamic pressure
r_α	dimensionless gyration radius of airfoil around stiffness center
t	real time
V_f^*	flutter speed index
$\mathbf{v}_i$	eigenvector associated with the ith eigenvalue of matrix
$\mathbf{v}_{im}$	imaginary part of the ith eigenvector
$\mathbf{v}_{ir}$	real part of the ith eigenvector
$\mathbf{x}_a$	state vector of aerodynamic state-space ROM
$\mathbf{x}_{as}$	state vector of aeroelastic state-space model
$\mathbf{x}_s$	state vector of structural state-space model

x_α	dimensionless distance of center of gravity behind stiffness center

Greek

α	pitch displacement
$\boldsymbol{\Gamma}_\theta$	feasible set of identified coefficients
$\boldsymbol{\Gamma}_\lambda$	feasible set of eigenvalues
δ	perturbation variable
Δ	radius of interval
$\boldsymbol{\theta}$	coefficient set of the aerodynamic ROM to be identified
$\hat{\boldsymbol{\theta}}$	estimation of identified coefficients
λ_i	the ith eigenvalue of matrix
λ_{im}	imaginary part of the ith eigenvalue of matrix
λ_{ir}	real part of the ith eigenvalue of matrix
μ	mass ratio
ν	Poisson's ratio
$\boldsymbol{\xi}$	system input (generalized structural displacement) vector
ρ	density
ω_h	uncoupled natural frequency of airfoil in plunge
ω_α	uncoupled natural frequency of airfoil in pitch

Abbreviations

ARMA	autoregressive moving average
ARX	autoregressive model with exogenous input
CFD	computational fluid dynamics
LB	lower bound
LTI	linear time invariant
MCS	Monte Carlo simulation
NV	nominal value
POD	proper orthogonal decomposition
ROM(s)	reduced-order model(s)
ROM-DAR	reduced-order modeling suitable for deterministic aerodynamic responses
ROM-UAR	reduced-order modeling suitable for uncertain aerodynamic responses
UB	upper bound

use in the conceptual design, control and data-driven systems [2]. According to different modeling ideas, the methodologies to reduce the order of an aerodynamic model can be subdivided broadly into two main categories: one is based on the proper orthogonal decomposition (POD) approach [3] and the other on the system identification technology, mainly including autoregressive moving average (ARMA) models [4], linear state-space models [5], Volterra series models [6] and neural networked models [7]. Typically, most of the current proposed CFD-based ROMs, such as first-order POD methods, ARMA models, linear state-space models and first-order Volterra series models, are dynamic linear models constructed under the assumption of small-amplitude vibrations, which can accurately predict mildly nonlinear responses and are suitable for a wide range of flight conditions. These aerodynamic ROMs have been extensively applied to the analysis or design of transonic flutter [8], limit cycle oscillation [9], gust response [10], aeroservoelasticity [11], aerothermoelasticity [12] and transonic flutter suppression with control delay [13] with respect to simple airfoils, three-dimensional wings and even complete aircrafts in both frequency and time domain through the years. Most of the existing aerodynamic ROMs are generally linear or weakly-nonlinear models. The latest developments in the field of aerodynamic model reduction especially nonlinear model reduction is discussed by Marques et

al. [14] Among the nonlinear ROMs, the nonlinear model projection is used to the reduction of nonlinear aerodynamic models for gust response prediction allowing a systematic investigation of the influence of a large number of gust shapes without regenerating the ROM [15]. The investigation on the accuracy of prediction and incurred computational cost of ROMs based on indicial functions, Volterra theory using nonlinear kernels, radial basis functions and a surrogate-based recurrence framework for X-31 aircraft pitching motions indicates that these ROMs can produce accurate predictions for a wide range of motions in transonic regime with a limited number of time-accurate CFD simulations [16]. While maintaining a high level of accuracy, the preceding aerodynamic model reduction methods can expedite the computational efficiency by 1 to 2 orders of magnitude compared with full CFD simulations, and demonstrate a huge potential for the analysis and design of aeroelasticity.

Generally, conventional aeroelasticity investigations are performed under the assumption of complete determinacy of systems. As a practical matter, real aeroelastic systems are inevitably confronted with multiple sources of uncertainty arising from 1) modeling-induced uncertainties due to simplifying assumptions, modal truncation, errors in boundary conditions and unmodeled dynamics, 2) numerical uncertainties generated by diversity in

mesh quality, different convergence precision and spatiotemporal discretization errors, 3) parametric uncertainties on account of inaccuracy or discrepancy of physical parameters involved in structural and aerodynamic subsystems. Theoretically, these aforementioned uncertainties will result in a significant impact on the aeroelastic behavior of concern. In current engineering field, the flutter margin is introduced to preclude the occurrence of aircraft flutter due to various uncertain factors throughout the flight envelope. This integrated estimation strategy for the uncertain factors lacks quantitative recognition to the uncertainty, which is contrary to the development tendency of precise and meticulous design for aeroelastic system and can even lead to a disastrous consequence. For instance, the insufficient estimation of uncertainty in aerodynamic modeling is one of the causes of inadequate control for hypersonic vehicle X-43A on its first test flight. Therefore, it is absolutely crucial to appropriately and accurately model the uncertain factors included in the aeroelastic system.

Typically, as reviewed by Pettit [17] and Dai et al. [18], uncertainty modeling for aeroelastic systems can be tackled by two major approaches, i.e. probabilistic and non-probabilistic methods, depending on distinct quantification techniques. The probabilistic methods, based on Monte Carlo simulation (MCS) [19], polynomial chaos expansion [20], stochastic collocation [21] and so on, have been prevalently employed to quantify the propagation of stochastic uncertainty through the aeroelastic system. These probabilistic approaches consider uncertainties as probabilistic variables and devote to achieving the adequate distribution characteristics of the aeroelastic stability boundary.

However, the main disadvantage of the probabilistic method is its over-reliance on the prior information of uncertainties, which is based on a large amount of experimental samples and is usually difficult to be obtained. Compared with the distribution information, the bounds of uncertain variables are easier to be defined. Hence, the non-probabilistic approaches including the interval theory [22], the perturbation technique and the structured singular value (μ) method [23], have emerged to deal with robust aeroelastic issues, in which the uncertain variables are described as bounded parameters and the "worst case" of the aeroelastic stability boundary throughout the uncertainty set is more concerned. Currently, most of the uncertainties embedded in robust aeroelastic analysis have been modeled in the physical parameter level for each subsystem. In terms of elastic structural subsystem, bounded damping and stiffness coefficients [24], weight uncertainty of the tip-mass together with its location variation [25], dispersivity of elastic modulus and density [26], and modal shape variations [27] were well modeled for comprehensive investigations into the influences of parametric changes in structure on robust aeroelastic stability boundary. As for aerodynamic subsystem, some attractive methods for uncertainty modeling of derivative of aerodynamic forces [28], aerodynamic influence coefficients [29], and unsteady aerodynamic pressure [30] were developed to evaluate the corresponding impacts on robust aeroelastic behavior. Additionally, uncertainties come from nonlinearity [31] and unmodeled dynamics [32] were also taken into account to conduct the robust aeroelastic stability analysis. It is noteworthy that there is still a long way to get an appropriate quantification of aerodynamic and nonlinear uncertainty and its contribution to aeroelastic instability compared with the structural uncertainty.

The robustness of the model reduction method, which describes the applicability of the ROM to aeroelastic systems with uncertainties, is also important in addition to accuracy and efficiency. In the aspect of research on CFD-based ROMs considering uncertainties, Lieu et al. [33] proposed a fast Mach-adaptation algorithm suitable for different freestream Mach numbers by angle interpolation between two POD subspaces. An efficient ROM robust to flight parameter variations was constructed by Liu et

al. [34] using Kriging surrogates and recurrence frameworks together in which the freestream Mach number is taken as a part of the input data. Zhang et al. [35] developed an aerodynamic model reduction method applicable for arbitrary structural modal shapes by the interpolation of basis generalized displacements. These improvements enhance the robustness and efficiency of the aerodynamic ROMs used in aeroelastic analysis. However, these improved ROMs address uncertainties by surrogate models or interpolation, and the models themselves are still deterministic in essence.

In addition, from the overall perspective, much of previous work in the robust aeroelasticity scope concentrates upon the parametric uncertainties existing in structural and aerodynamic subsystems while aerodynamic responses produced by the CFD solver are regularly considered deterministic. In fact, CFD simulation has the nature of approximation and dispersion, and always accompanied by multiple sources of uncertainty. As NASA's technical vision [36] of the required capabilities of CFD in the notional year 2030 indicates, management of uncertainty quantification and propagation in CFD simulation is regarded as a bottleneck to be conquered to improve the credibility of predictions. Although numerous types of uncertainties associated with CFD simulations originating from discretization errors [37], different turbulence models, uncertain initial or boundary data [38] and so on have been exclusively investigated, research on aerodynamic reduced-order modeling considering the CFD-induced uncertainties and further application in robust aeroelastic analysis is still in its preliminary stage.

Hence, the motivation for this paper is to develop a CFD-based model reduction strategy for unsteady aerodynamics considering bounded uncertainties associated with CFD simulation and simultaneously promote its application into robust flutter boundary prediction. For this purpose, the interval perturbation method is proposed to get the interval estimation of identified coefficients in the uncertain aerodynamic reduced-order model and eigenvalues of the uncertain aeroelastic state matrix. The remainder of this paper is organized as follows. In section 2, an uncertain model reduction method for aerodynamic subsystems with interval parameters is developed based on the system identification theory and the first-order interval perturbation approach. In section 3, a strategy to predict the robust flutter boundary of the formulated uncertain aeroelastic model is proposed with the help of the standard interval eigenvalue solving algorithm and the newly defined stability criterion about the interval aeroelastic state matrix. Two numerical examples are given to demonstrate the validity and accuracy of the presented uncertain aerodynamic model reduction method as well as the robust flutter analysis approach in section 4. Finally, some conclusions are summarized in section 5.

2. Uncertain reduced-order modeling for aerodynamic subsystems with interval parameters

In the current section, an uncertain model reduction method based on the system identification approach is proposed for aerodynamic subsystems where CFD-induced bounded uncertainties of aerodynamic responses are considered. The interval estimation of identified coefficients of the reduced-order model is obtained by utilizing the first-order interval perturbation theory. Above all, the conventional strategy for aerodynamic reduced-order modeling applied in the field of transonic flutter analysis and optimization is briefly introduced.

2.1. Reduced-order modeling suitable for deterministic aerodynamic responses (ROM-DAR)

Model reduction procedures are widely used in aeroelastic stability prediction to improve the computational efficiency of the unsteady CFD solution in transonic regime. Conceptually, the unsteady CFD solution performed in an aeroelastic analysis is simply a dynamic system that calculates the aerodynamic responses based on a prescribed motion of the structure. For an aeroelastic stability problem involving structural vibrations with small amplitude only, the aerodynamic subsystem can be assumed to be a dynamic linear system. Under this assumption, although the steady flow fields are nonlinear in spatial dimension, the unsteady aerodynamic responses are considered to be linear with regard to small-amplitude vibrations of structure in temporal dimension. Hence, based on the dynamic linearization hypothesis, the aerodynamic subsystem can be regarded as a linear time invariant (LTI) system with multiple inputs and multiple outputs. Multiple forms of unsteady aerodynamic ROMs have been developed to mathematically describe the input/output relationship of the unsteady CFD solution.

In the current investigation, the ARX (AutoRegressive model with eXogenous input) model is adopted to construct the unsteady aerodynamic ROM based on the system identification method. In the process of aerodynamic model reduction, the multistep signal with a broad spectrum of frequencies is used as the mode excitations (generalized structural displacements) to excite the primary flow physics, and the CFD solver is employed to generate the aerodynamic responses (generalized aerodynamic coefficients based on the normal mode shapes) corresponding to the prescribed mode excitations in discrete-time domain. The ARX model describes the responses of the investigated aerodynamic subsystem as a sum of scaled previous outputs and scaled present and previous inputs, which can be written as [35]

$$\mathbf{f}(k) = \sum_{i=1}^{na} \mathbf{A}_i \mathbf{f}(k-i) + \sum_{j=0}^{nb-1} \mathbf{B}_j \boldsymbol{\xi}(k-j) + \mathbf{e}(k) \tag{1}$$

where $\mathbf{f}(k)$ is the kth data of the M-dimensional vector of system outputs (generalized aerodynamic coefficients), and $\boldsymbol{\xi}(k)$ denotes the kth data of the M-dimensional vector of system inputs (generalized structural displacements). M is the modal truncation order of the structural subsystem. $\mathbf{A}_i$ and $\mathbf{B}_j$ are the coefficient matrices to be identified. na and nb are delay orders of outputs and inputs, respectively. $\mathbf{e}(k)$ represents the kth data of model output errors corresponding to the original system outputs. In terms of deterministic aerodynamic responses, the unknown model coefficients in Eq. (1) are deterministic and can be estimated using the least squares method. Thus, the unsteady aerodynamic ROM suitable for deterministic aerodynamic responses is constructed.

2.2. Reduced-order modeling suitable for uncertain aerodynamic responses (ROM-UAR)

Due to the complexity of the aerodynamic subsystem, the aerodynamic responses generated by the CFD solver are inevitably confronted with the influence of uncertainties originating from errors or diversities of boundary conditions, mesh sizes, spatiotemporal discretization and other sources. Apparently, in order to make confident predictions of the concerned aerodynamic subsystem, the consideration of uncertainties involved in aerodynamic responses becomes indispensable and the presented deterministic model reduction method needs to be improved accordingly. Since most uncertainty quantification schemes are based on the description of the uncertainties as random variables, the probabilistic method becomes the preferred way to deal with uncertain problems. However, the probabilistic technique requires sufficient sample infor-

mation to acquire the probability density functions of uncertainties, which will consequentially lead to extremely large CFD computational costs for the current uncertainty quantification problem of aerodynamic responses. Generally, compared with the distribution information, the bounds of uncertain variables can be attained more conveniently. In this paper, considering the actual situation that the available information of uncertainties of aerodynamic responses $\mathbf{f}(k) = (f_i(k)), i = 1, 2, \ldots, M$ is not sufficient to provide the probability density function, each element of the kth aerodynamic response vector $\mathbf{f}(k)$ is assumed to belong to an interval number. Thus, the uncertain aerodynamic ROM considering interval uncertainties of aerodynamic responses can be described as the following perturbed form

$$\mathbf{f}^c(k) + \delta\mathbf{f}(k) = \sum_{i=1}^{na} \mathbf{A}_i \big(\mathbf{f}^c(k-i) + \delta\mathbf{f}(k-i) \big)$$
$$+ \sum_{j=0}^{nb-1} \mathbf{B}_j \boldsymbol{\xi}(k-j) + \mathbf{e}(k) \tag{2}$$

where $\mathbf{f}^c(k)$ stands for the nominal value of the kth vector of system outputs and can be regarded as the deterministic part of the generalized aerodynamic response vector. $\delta\mathbf{f}(k) \in \Delta\mathbf{f}^I(k)$ is a small perturbation from $\mathbf{f}^c(k)$ and can be considered as the uncertain part of the generalized aerodynamic response vector. $\Delta\mathbf{f}^I(k) = [-\Delta\mathbf{f}(k), \Delta\mathbf{f}(k)]$ denotes the interval of the uncertain part of the generalized aerodynamic response vector with zero nominal value where $\Delta\mathbf{f}(k) = (\Delta f_i(k)), i = 1, 2, \ldots, M$ is the radius of the interval vector $\Delta\mathbf{f}^I(k)$.

For convenience, Eq. (2) can be rewritten as the least squares scheme for inputs and outputs of the investigated system as below

$$\mathbf{f}^c(k) + \delta\mathbf{f}(k) = \boldsymbol{\theta}^T \big(\mathbf{x}^c(k) + \delta\mathbf{x}(k) \big) + \mathbf{e}(k) \tag{3}$$

where $\boldsymbol{\theta}^T = [\mathbf{A}_1 \cdots \mathbf{A}_{na} \mathbf{B}_0 \cdots \mathbf{B}_{nb-1}]$ is a $M \times (na + nb) \cdot M$-dimensional coefficient set of aerodynamic ROM to be identified. $\mathbf{x}^c(k) = [(\mathbf{f}^c(k-1))^T, \ldots, (\mathbf{f}^c(k-na))^T, \boldsymbol{\xi}^T(k), \ldots, \boldsymbol{\xi}^T(k-nb+1)]^T$ and $\delta\mathbf{x}(k) = [(\delta\mathbf{f}(k-1))^T, \ldots, (\delta\mathbf{f}(k-na))^T, \mathbf{0}, \ldots, \mathbf{0}]^T \in \Delta\mathbf{x}^I(k)$ represent the nominal value of a $(na + nb) \cdot M$-dimensional vector of inputs and outputs, and a small perturbation around $\mathbf{x}^c(k)$, respectively.

Taking L as the data length of system inputs and outputs in the process of identification, namely $k = 1, 2, \ldots, L$, we can obtain the following identification format with the help of Eq. (3)

$$\mathbf{F}_L^c + \delta\mathbf{F}_L = \big(\mathbf{H}_L^c + \delta\mathbf{H}_L \big) \boldsymbol{\theta} + \mathbf{E}_L \tag{4}$$

where

$$\mathbf{F}_L^c = \begin{bmatrix} (\mathbf{f}^c(1))^T \\ (\mathbf{f}^c(2))^T \\ \vdots \\ (\mathbf{f}^c(L))^T \end{bmatrix}, \qquad \delta\mathbf{F}_L = \begin{bmatrix} (\delta\mathbf{f}(1))^T \\ (\delta\mathbf{f}(2))^T \\ \vdots \\ (\delta\mathbf{f}(L))^T \end{bmatrix} \in \Delta\mathbf{F}_L^I,$$

$$\mathbf{E}_L = \begin{bmatrix} \mathbf{e}^T(1) \\ \mathbf{e}^T(2) \\ \vdots \\ \mathbf{e}^T(L) \end{bmatrix}$$

$$\mathbf{H}_L^c = \begin{bmatrix} (\mathbf{x}^c(1))^T \\ (\mathbf{x}^c(2))^T \\ \vdots \\ (\mathbf{x}^c(L))^T \end{bmatrix}$$

$$= \begin{bmatrix} (\mathbf{f}^c(0))^T & \cdots & (\mathbf{f}^c(1-na))^T & \boldsymbol{\xi}^T(1) & \cdots & \boldsymbol{\xi}^T(2-nb) \\ (\mathbf{f}^c(1))^T & \cdots & (\mathbf{f}^c(2-na))^T & \boldsymbol{\xi}^T(2) & \cdots & \boldsymbol{\xi}^T(3-nb) \\ \vdots & \ddots & \vdots & \vdots & \ddots & \vdots \\ (\mathbf{f}^c(L-1))^T & \cdots & (\mathbf{f}^c(L-na))^T & \boldsymbol{\xi}^T(L) & \cdots & \boldsymbol{\xi}^T(L+1-nb) \end{bmatrix}$$

$$\delta\mathbf{H}_L = \begin{bmatrix} (\delta\mathbf{x}(1))^T \\ (\delta\mathbf{x}(2))^T \\ \vdots \\ (\delta\mathbf{x}(L))^T \end{bmatrix} \tag{5}$$

$$= \begin{bmatrix} (\delta\mathbf{f}(0))^T & \cdots & (\delta\mathbf{f}(1-na))^T & \mathbf{0} & \cdots & \mathbf{0} \\ (\delta\mathbf{f}(1))^T & \cdots & (\delta\mathbf{f}(2-na))^T & \mathbf{0} & \cdots & \mathbf{0} \\ \vdots & \ddots & \vdots & \vdots & \ddots & \vdots \\ (\delta\mathbf{f}(L-1))^T & \cdots & (\delta\mathbf{f}(L-na))^T & \mathbf{0} & \cdots & \mathbf{0} \end{bmatrix}$$

$$\in \Delta\mathbf{H}_L^I$$

Basing on the principle of least squares method, we can define the criterion function as below

$$J(\boldsymbol{\theta}) = \sum_{k=1}^L \mathbf{e}^T(k)\mathbf{e}(k) = \|\mathbf{F}_L - \mathbf{H}_L\boldsymbol{\theta}\|_F^2$$
$$= \operatorname{tr}\big((\mathbf{F}_L - \mathbf{H}_L\boldsymbol{\theta})^T(\mathbf{F}_L - \mathbf{H}_L\boldsymbol{\theta})\big) \tag{6}$$

where $\|\bullet\|_F$ denotes the Frobenius-norm of a matrix, $\mathbf{F}_L = \mathbf{F}_L^c + \delta\mathbf{F}_L$ and $\mathbf{H}_L = \mathbf{H}_L^c + \delta\mathbf{H}_L$.

Eq. (6) clearly characterizes the error of the aerodynamic ROM compared with the original CFD solver. By minimizing the criterion function (6), we can get the estimated value $\hat{\boldsymbol{\theta}}$ of coefficients involved in Eq. (4) which satisfies

$$\nabla_{\boldsymbol{\theta}} J(\boldsymbol{\theta})\big|_{\hat{\boldsymbol{\theta}}} = \nabla_{\boldsymbol{\theta}}\big(\operatorname{tr}(\mathbf{F}_L^T\mathbf{F}_L) - 2\operatorname{tr}(\mathbf{F}_L^T\mathbf{H}_L\boldsymbol{\theta}) + \operatorname{tr}(\boldsymbol{\theta}^T\mathbf{H}_L^T\mathbf{H}_L\boldsymbol{\theta})\big)\big|_{\hat{\boldsymbol{\theta}}}$$
$$= 2\big(-\mathbf{H}_L^T\mathbf{F}_L + \mathbf{H}_L^T\mathbf{H}_L\hat{\boldsymbol{\theta}}\big) = \mathbf{0} \tag{7}$$

where $\nabla_{\boldsymbol{\theta}}(\bullet)$ stands for the derivative of a scalar quantity with respect to a matrix expressed as

$$\nabla_{\boldsymbol{\theta}} = \begin{bmatrix} \frac{\partial}{\partial\theta_{11}} & \frac{\partial}{\partial\theta_{12}} & \cdots & \frac{\partial}{\partial\theta_{1j}} \\ \frac{\partial}{\partial\theta_{21}} & \frac{\partial}{\partial\theta_{22}} & \cdots & \frac{\partial}{\partial\theta_{2j}} \\ \vdots & \vdots & \ddots & \vdots \\ \frac{\partial}{\partial\theta_{i1}} & \frac{\partial}{\partial\theta_{i2}} & \cdots & \frac{\partial}{\partial\theta_{ij}} \end{bmatrix},$$
$$i = 1, 2, \ldots, (na+nb)\cdot M; \quad j = 1, 2, \ldots, M \tag{8}$$

Due to the uncertainties involved in the systemic outputs (aerodynamic responses) $\mathbf{f}(k)$, the estimation of identified coefficients $\hat{\boldsymbol{\theta}}$ determined by inputs and outputs of the system are also uncertain. With the idea of least squares method, the critical job for reduced-order modeling of the uncertain aerodynamic subsystem of interest is to seek a feasible set $\boldsymbol{\Gamma_\theta} \subset \mathbf{R}^{(na+nb)\cdot M \times M}$ of the uncertain coefficient matrices $\hat{\boldsymbol{\theta}}$ which is compatible with the mode excitations and bounded aerodynamic responses, namely

$$\boldsymbol{\Gamma_\theta} = \big\{ \hat{\boldsymbol{\theta}} : -\mathbf{H}_L^T\big(\delta\mathbf{f}(k)\big)\mathbf{F}_L\big(\delta\mathbf{f}(k)\big) + \mathbf{H}_L^T\big(\delta\mathbf{f}(k)\big)\mathbf{H}_L\big(\delta\mathbf{f}(k)\big)\hat{\boldsymbol{\theta}} = \mathbf{0},$$
$$\delta\mathbf{f}(k) \in \Delta\mathbf{f}^I(k) \big\} \tag{9}$$

In general, $\boldsymbol{\Gamma_\theta}$ is an irregular convex set with a complicated boundary which is particularly difficult and unnecessary to find out. For facilitating system analysis and control, a convex set, which is easy handling and contains the feasible set $\boldsymbol{\Gamma_\theta}$ as tightly as possible is expected. By virtue of interval mathematics, we can seek a hyper-rectangle (or interval matrix) to approximate set $\boldsymbol{\Gamma_\theta}$. That is to say, the interval estimation of $\boldsymbol{\Gamma_\theta}$ can be obtained by determining the lower and upper bounds of the system coefficient matrices as follows

$$\hat{\boldsymbol{\theta}}^I = \big[\underline{\hat{\boldsymbol{\theta}}}\big(\delta\mathbf{f}(k)\big), \bar{\hat{\boldsymbol{\theta}}}\big(\delta\mathbf{f}(k)\big)\big] = \big(\hat{\theta}_{ij}^I\big(\delta\mathbf{f}(k)\big)\big) \tag{10}$$

where

$$\underline{\hat{\boldsymbol{\theta}}}\big(\delta\mathbf{f}(k)\big) = \min\big\{\hat{\boldsymbol{\theta}} : -\mathbf{H}_L^T\big(\delta\mathbf{f}(k)\big)\mathbf{F}_L\big(\delta\mathbf{f}(k)\big) + \mathbf{H}_L^T\big(\delta\mathbf{f}(k)\big)\mathbf{H}_L\big(\delta\mathbf{f}(k)\big)\hat{\boldsymbol{\theta}} = \mathbf{0}, \delta\mathbf{f}(k) \in \Delta\mathbf{f}^I(k)\big\}$$
$$\bar{\hat{\boldsymbol{\theta}}}\big(\delta\mathbf{f}(k)\big) = \max\big\{\hat{\boldsymbol{\theta}} : -\mathbf{H}_L^T\big(\delta\mathbf{f}(k)\big)\mathbf{F}_L\big(\delta\mathbf{f}(k)\big) + \mathbf{H}_L^T\big(\delta\mathbf{f}(k)\big)\mathbf{H}_L\big(\delta\mathbf{f}(k)\big)\hat{\boldsymbol{\theta}} = \mathbf{0}, \delta\mathbf{f}(k) \in \Delta\mathbf{f}^I(k)\big\} \tag{11}$$

We assume that the estimation of the identified coefficients $\hat{\boldsymbol{\theta}}$ has the following form

$$\hat{\boldsymbol{\theta}} = \hat{\boldsymbol{\theta}}^c + \delta\hat{\boldsymbol{\theta}} \tag{12}$$

where $\hat{\boldsymbol{\theta}}^c$ and $\delta\hat{\boldsymbol{\theta}} \in \Delta\hat{\boldsymbol{\theta}}^I$ stand for the nominal estimation of identified coefficients and a small perturbation from $\hat{\boldsymbol{\theta}}^c$, respectively. $\Delta\hat{\boldsymbol{\theta}}^I = [-\Delta\hat{\boldsymbol{\theta}}, \Delta\hat{\boldsymbol{\theta}}]$ is the interval of the uncertain part of the identified coefficient matrix with zero nominal value where $\Delta\hat{\boldsymbol{\theta}} = (\Delta\hat{\theta}_{ij}), i = 1, 2, \ldots, (na+nb)\cdot M; j = 1, 2, \ldots, M$ is the radius of the interval matrix $\Delta\hat{\boldsymbol{\theta}}^I$. Substituting Eq. (12) into Eq. (7) yields

$$-\big(\mathbf{H}_L^c + \delta\mathbf{H}_L\big)^T\big(\mathbf{F}_L^c + \delta\mathbf{F}_L\big) + \big(\mathbf{H}_L^c + \delta\mathbf{H}_L\big)^T\big(\mathbf{H}_L^c + \delta\mathbf{H}_L\big)\big(\hat{\boldsymbol{\theta}}^c + \delta\hat{\boldsymbol{\theta}}\big) = \mathbf{0} \tag{13}$$

Expanding Eq. (13) and neglecting the higher-order terms, we have

$$\hat{\boldsymbol{\theta}}^c = \big((\mathbf{H}_L^c)^T\mathbf{H}_L^c\big)^{-1}(\mathbf{H}_L^c)^T\mathbf{F}_L^c$$
$$\delta\hat{\boldsymbol{\theta}} = \big((\mathbf{H}_L^c)^T\mathbf{H}_L^c\big)^{-1}\big((\mathbf{H}_L^c)^T\delta\mathbf{F}_L + (\delta\mathbf{H}_L)^T\mathbf{F}_L^c - (\mathbf{H}_L^c)^T\delta\mathbf{H}_L\hat{\boldsymbol{\theta}}^c - (\delta\mathbf{H}_L)^T\mathbf{H}_L^c\hat{\boldsymbol{\theta}}^c\big) \tag{14}$$

where $\delta\hat{\boldsymbol{\theta}}$ can be regarded as a function of the elements in $\delta\mathbf{H}_L$ and $\delta\mathbf{F}_L$. By means of the principle of interval mathematics, we can obtain the interval natural extension of the second equation in Eq. (14) as

$$\Delta\hat{\boldsymbol{\theta}} = \sum_{i=1}^M \sum_{k=1}^L \Big| \big((\mathbf{H}_L^c)^T\mathbf{H}_L^c\big)^{-1}\Big((\mathbf{H}_L^c)^T\frac{\partial\mathbf{F}_L^c}{\partial f_i(k)} + \Big(\frac{\partial\mathbf{H}_L^c}{\partial f_i(k)}\Big)^T\mathbf{F}_L^c$$
$$- (\mathbf{H}_L^c)^T\frac{\partial\mathbf{H}_L^c}{\partial f_i(k)}\hat{\boldsymbol{\theta}}^c - \Big(\frac{\partial\mathbf{H}_L^c}{\partial f_i(k)}\Big)^T\mathbf{H}_L^c\hat{\boldsymbol{\theta}}^c\Big)\Big| \Delta f_i(k) \tag{15}$$

By virtue of the first equation in Eq. (14) and Eq. (15), the lower and upper bounds of identified coefficients $\hat{\boldsymbol{\theta}}$ used as the interval estimation of $\boldsymbol{\Gamma_\theta}$ can be readily obtained via interval operations

$$\hat{\boldsymbol{\theta}}^I = \hat{\boldsymbol{\theta}}^c + \Delta\hat{\boldsymbol{\theta}}^I = [\underline{\hat{\boldsymbol{\theta}}}, \bar{\hat{\boldsymbol{\theta}}}] = [\hat{\boldsymbol{\theta}}^c - \Delta\hat{\boldsymbol{\theta}}, \hat{\boldsymbol{\theta}}^c + \Delta\hat{\boldsymbol{\theta}}] \tag{16}$$

Eq. (16) can also be written as the component form

$$\hat{\theta}_{ij} = \hat{\theta}_{ij}^c + \Delta\hat{\theta}_{ij}^I = [\underline{\hat{\theta}}_{ij}, \bar{\hat{\theta}}_{ij}] = [\hat{\theta}_{ij}^c - \Delta\hat{\theta}_{ij}, \hat{\theta}_{ij}^c + \Delta\hat{\theta}_{ij}],$$
$$i = 1, 2, \ldots, (na+nb)\cdot M; \quad j = 1, 2, \ldots, M \tag{17}$$

It is worth noting that the proposed method is limited to the case where the CFD-induced uncertainties of aerodynamic responses are small since only the first-order perturbation is employed in Eq. (14). However, for the situation that the uncertainties of the concerned aerodynamic responses are large, the second-order perturbation in Eq. (13) should be taken into consideration.

Then, with the help of Eq. (14) to Eq. (17), the uncertain aerodynamic ROM considering interval uncertainties of aerodynamic responses can be constructed as follows

$$\mathbf{f}(k) = \left(\hat{\boldsymbol{\theta}}^I\right)^T \mathbf{x}(k) = \sum_{i=1}^{na} \mathbf{A}_i^I \mathbf{f}(k-i) + \sum_{j=0}^{nb-1} \mathbf{B}_i^I \boldsymbol{\xi}(k-j) \tag{18}$$

It is obvious that the coefficient matrices of the above reduced-order model are interval matrices rather than deterministic matrices. The proposed reduced-order model with interval uncertainties can be used to predict uncertain responses of the aerodynamic subsystem where CFD-induced uncertainties are considered and replace the CFD solver for the aeroelastic uncertainty analysis in transonic regime.

3. Robust flutter analysis based on the aerodynamic ROM in presence of interval uncertainties

In this section, the stability problem of an uncertain aeroelastic state-space model with interval parameters is transformed into a standard interval eigenvalue problem associated with a real non-symmetric interval matrix. The lower and upper bounds of eigenvalues of the uncertain aeroelastic state matrix are evaluated by virtue of the first-order interval matrix perturbation algorithm. By reference to the Lyapunov stability criterion for deterministic situations, a new stability criterion with respect to the interval aeroelastic continuous-time state-space model is defined to predict the robust flutter boundary of the investigated uncertain aeroelastic system. Primarily, the state-space model of the uncertain aeroelastic system is formulated by coupling the above proposed uncertain aerodynamic ROM with the structural dynamic equation in continuous-time domain.

3.1. Aeroelastic state-space model construction based on the uncertain ROM

For the convenience of the subsequent aeroelastic stability analysis, the difference model of the uncertain aerodynamic ROM described by Eq. (18) should be transformed into the state-space form. Here, we define a state vector $\mathbf{x}_a(k)$ consisting of vectors of generalized aerodynamic coefficients and generalized structural displacements as follows

$$\mathbf{x}_a(k) = \left[\mathbf{f}^T(k-1), \dots, \mathbf{f}^T(k-na), \boldsymbol{\xi}^T(k-1), \dots, \right.$$
$$\left. \boldsymbol{\xi}^T(k-nb+1)\right]^T \tag{19}$$

Then, the state-space form of the uncertain aerodynamic ROM in discrete-time domain can be expressed as

$$\mathbf{x}_a(k+1) = \tilde{\mathbf{A}}_a^I \mathbf{x}_a(k) + \tilde{\mathbf{B}}_a^I \boldsymbol{\xi}(k)$$
$$\mathbf{f}(k) = \tilde{\mathbf{C}}_a^I \mathbf{x}_a(k) + \tilde{\mathbf{D}}_a^I \boldsymbol{\xi}(k) \tag{20}$$

where

$$\tilde{\mathbf{A}}_a^I = \begin{bmatrix} \mathbf{A}_1^I & \mathbf{A}_2^I & \cdots & \mathbf{A}_{na-1}^I & \mathbf{A}_{na}^I & \mathbf{B}_1^I & \mathbf{B}_2^I & \cdots & \mathbf{B}_{nb-2}^I & \mathbf{B}_{nb-1}^I \\ \mathbf{I} & \mathbf{0} & \cdots & \mathbf{0} & \mathbf{0} & \mathbf{0} & \mathbf{0} & \cdots & \mathbf{0} & \mathbf{0} \\ \mathbf{0} & \mathbf{I} & \cdots & \mathbf{0} & \mathbf{0} & \mathbf{0} & \mathbf{0} & \cdots & \mathbf{0} & \mathbf{0} \\ \vdots & \vdots & \ddots & \vdots & \vdots & \vdots & \vdots & \ddots & \vdots & \vdots \\ \mathbf{0} & \mathbf{0} & \cdots & \mathbf{I} & \mathbf{0} & \mathbf{0} & \mathbf{0} & \cdots & \mathbf{0} & \mathbf{0} \\ \mathbf{0} & \mathbf{0} & \cdots & \mathbf{0} & \mathbf{0} & \mathbf{0} & \mathbf{0} & \cdots & \mathbf{0} & \mathbf{0} \\ \mathbf{0} & \mathbf{0} & \cdots & \mathbf{0} & \mathbf{0} & \mathbf{I} & \mathbf{0} & \cdots & \mathbf{0} & \mathbf{0} \\ \mathbf{0} & \mathbf{0} & \cdots & \mathbf{0} & \mathbf{0} & \mathbf{0} & \mathbf{I} & \cdots & \mathbf{0} & \mathbf{0} \\ \vdots & \vdots & \ddots & \vdots & \vdots & \vdots & \vdots & \ddots & \vdots & \vdots \\ \mathbf{0} & \mathbf{0} & \cdots & \mathbf{0} & \mathbf{0} & \mathbf{0} & \mathbf{0} & \cdots & \mathbf{I} & \mathbf{0} \end{bmatrix} \tag{21}$$

$$\tilde{\mathbf{B}}_a^I = \left[(\mathbf{B}_0^I)^T \quad \mathbf{0} \quad \mathbf{0} \quad \cdots \quad \mathbf{0} \quad \mathbf{I} \quad \mathbf{0} \quad \mathbf{0} \quad \cdots \quad \mathbf{0} \right]^T$$

$$\tilde{\mathbf{C}}_a^I = [\mathbf{A}_1^I \quad \mathbf{A}_2^I \quad \cdots \quad \mathbf{A}_{na-1}^I \quad \mathbf{A}_{na}^I \quad \mathbf{B}_1^I \quad \mathbf{B}_2^I$$
$$\cdots \quad \mathbf{B}_{nb-2}^I \quad \mathbf{B}_{nb-1}^I]$$

$$\tilde{\mathbf{D}}_a^I = [\mathbf{B}_0^I]$$

To couple the structural equations in continuous-time domain, the discrete-time state-space form of the uncertain aerodynamic ROM is further converted to the continuous-time form as

$$\dot{\mathbf{x}}_a(t) = \mathbf{A}_a^I \mathbf{x}_a(t) + \mathbf{B}_a^I \boldsymbol{\xi}(t)$$
$$\mathbf{f}(t) = \mathbf{C}_a^I \mathbf{x}_a(t) + \mathbf{D}_a^I \boldsymbol{\xi}(t) \tag{22}$$

Now, consider the following continuous-time structural dynamic equation in the modal basis coordinates

$$\mathbf{M}\ddot{\boldsymbol{\xi}}(t) + \mathbf{G}\dot{\boldsymbol{\xi}}(t) + \mathbf{K}\boldsymbol{\xi}(t) = \mathbf{F}(t) \tag{23}$$

where $\mathbf{M}$ represents the generalized mass matrix, $\mathbf{G}$ is the generalized damping matrix, $\mathbf{K}$ denotes the generalized stiffness matrix, and $\mathbf{F}(t) = q\mathbf{f}(t)$ is the generalized aerodynamic force vector, where q is the dynamic pressure of the freestream. By introducing state vector $\mathbf{x}_s = [\boldsymbol{\xi}^T, \dot{\boldsymbol{\xi}}^T]^T$, the continuous-time state-space form of the structural dynamic equation is as follows

$$\dot{\mathbf{x}}_s(t) = \mathbf{A}_s \cdot \mathbf{x}_s(t) + q \cdot \mathbf{B}_s \cdot \mathbf{f}(t)$$
$$\boldsymbol{\xi}(t) = \mathbf{C}_s \cdot \mathbf{x}_s(t) + q \cdot \mathbf{D}_s \cdot \mathbf{f}(t) \tag{24}$$

where the system parameter matrices in Eq. (24) are respectively written as

$$\mathbf{A}_s = \begin{bmatrix} \mathbf{0} & \mathbf{I} \\ -\mathbf{M}^{-1}\mathbf{K} & -\mathbf{M}^{-1}\mathbf{G} \end{bmatrix}, \qquad \mathbf{B}_s = \begin{bmatrix} \mathbf{0} \\ \mathbf{M}^{-1} \end{bmatrix},$$
$$\mathbf{C}_s = \begin{bmatrix} \mathbf{I} & \mathbf{0} \end{bmatrix}, \qquad \mathbf{D}_s = [\mathbf{0}] \tag{25}$$

Coupling the state-space equations of the uncertain aerodynamic ROM described by Eq. (20) with the structural dynamic state-space equations expressed by Eq. (24) in continuous-time domain, the state-space model for the uncertain aeroelastic system in presence of interval parameters can be constructed as

$$\begin{bmatrix} \dot{\mathbf{x}}_s(t) \\ \dot{\mathbf{x}}_a(t) \end{bmatrix} = \begin{bmatrix} \mathbf{A}_s + q\mathbf{B}_s\mathbf{D}_a^I\mathbf{C}_s & q\mathbf{B}_s\mathbf{C}_a^I \\ \mathbf{B}_a^I\mathbf{C}_s & \mathbf{A}_a^I \end{bmatrix} \begin{bmatrix} \mathbf{x}_s(t) \\ \mathbf{x}_a(t) \end{bmatrix}$$

$$\boldsymbol{\xi}(t) = \begin{bmatrix} \mathbf{C}_s & \mathbf{0} \end{bmatrix} \begin{bmatrix} \mathbf{x}_s(t) \\ \mathbf{x}_a(t) \end{bmatrix} \tag{26}$$

To simplify the representation, assume that

$$\mathbf{x}_{as}(t) = \begin{bmatrix} \mathbf{x}_s(t) \\ \mathbf{x}_a(t) \end{bmatrix}, \qquad \mathbf{A}_{as}^I = \begin{bmatrix} \mathbf{A}_s + q\mathbf{B}_s\mathbf{D}_a^I\mathbf{C}_s & q\mathbf{B}_s\mathbf{C}_a^I \\ \mathbf{B}_a^I\mathbf{C}_s & \mathbf{A}_a^I \end{bmatrix},$$
$$\mathbf{C}_{as} = \begin{bmatrix} \mathbf{C}_s & \mathbf{0} \end{bmatrix} \tag{27}$$

Then, Eq. (26) can be rewritten as

$$\dot{\mathbf{x}}_{as}(t) = \mathbf{A}_{as}^I \mathbf{x}_{as}(t)$$
$$\boldsymbol{\xi}(t) = \mathbf{C}_{as}\mathbf{x}_{as}(t) \tag{28}$$

Up to present, the continuous-time state-space model of the uncertain aeroelastic system with interval parameters has been formulated. As compared with the conventional deterministic aeroelastic system, the state matrix $\mathbf{A}_{as}^l$ of the uncertain aeroelastic system described by Eq. (28) is composed of interval parameters, which reflects the influence of uncertainties involved in the aerodynamic subsystem. How to evaluate the stability and predict the flutter boundary of an uncertain aeroelastic system with interval parameters becomes an appealing problem, which will be discussed in the next subsection.

3.2. Robust flutter boundaries prediction for interval aeroelastic state-space model

The stability of a given aeroelastic system is directly related to the eigenvalues of the state matrix of the corresponding aeroelastic state-space model. Lyapunov stability analysis approach has been widely applied to evaluate the stability of a conventional aeroelastic state-space model with deterministic parameters. In terms of practice, Lyapunov stability condition is equivalent to the eigenvalues criterion. Due to the coupling of aerodynamics and structures destroying the symmetry of the structural subsystem, the eigenvalues of the state matrix of the aeroelastic system are complex numbers. In accordance with Lyapunov stability condition, an aeroelastic system is considered to be stable in continuous-time domain only if all the eigenvalues of the state matrix of the aeroelastic state-space model are absolutely distributed in the left-half complex plane.

However, for a given dynamic pressure q, the state matrix $\mathbf{A}_{as}^l$ in Eq. (28) now is an interval matrix, that leads to the real and imaginary parts of its eigenvalues are also interval numbers. By reference to the Lyapunov stability criterion suitable for deterministic cases, we can define the stability criterion with respect to the uncertain aeroelastic state-space model with interval parameters in continuous-time domain as follows: for any state matrix $\mathbf{A}_{as} \in \mathbf{A}_{as}^l$, if all the eigenvalues of $\mathbf{A}_{as}$ are distributed in the left-half complex plane, then the interval aeroelastic system is robustly stable; assume that we can find two different state matrices $\mathbf{A}_{as}$ and $\mathbf{A}_{as}'$ belonging to $\mathbf{A}_{as}^l$, if all the eigenvalues of $\mathbf{A}_{as}$ are distributed in the left-half complex plane while some of the eigenvalues of $\mathbf{A}_{as}'$ are distributed in the right-half complex plane (real axis included), then the interval aeroelastic system is possibly stable; for any state matrix $\mathbf{A}_{as} \in \mathbf{A}_{as}^l$, if all the eigenvalues of $\mathbf{A}_{as}$ are distributed in the right-half complex plane (real axis included), then the interval aeroelastic system is absolutely unstable.

Evidently, in order to achieve the distribution information of eigenvalues of the concerned interval state matrix, we should acquire the lower and upper bounds of the corresponding eigenvalues in advance. In particular, the stability problem of an uncertain aeroelastic state-space model here is transformed into a standard interval eigenvalue problem associated with a real non-symmetric $n \times n (n = (na + na + 1) \cdot M)$ interval matrix as below

$$\mathbf{A}_{as}^l \boldsymbol{v} = \left(\mathbf{A}_{as}^c + \Delta\mathbf{A}_{as}^l\right)\boldsymbol{v} = \lambda \boldsymbol{v} \tag{29}$$

where $\mathbf{A}_{as}^c$ denotes the nominal value of $\mathbf{A}_{as}^l$, $\Delta\mathbf{A}_{as}^l = [-\Delta\mathbf{A}_{as}, \Delta\mathbf{A}_{as}]$ is the interval of the uncertain part of the state matrix with zero nominal value where $\Delta\mathbf{A}_{as}$ is the radius matrix of $\mathbf{A}_{as}^l$, λ is the eigenvalue of $\mathbf{A}_{as}^l$ and $\boldsymbol{v}$ is the associated eigenvector. All the possible eigenvalues satisfying Eq. (29) constitute a feasible region in complex number field C which can be denoted by

$$\boldsymbol{\Gamma}_\lambda = \left\{\lambda : \lambda \in \mathbb{C}, \mathbf{A}_{as}^l \boldsymbol{v} = \lambda \boldsymbol{v}, \mathbf{A}_{as} \in \mathbf{A}_{as}^l\right\} \tag{30}$$

In view of the boundary complexity of the set $\boldsymbol{\Gamma}_\lambda$, we tend to seek an interval vector, which can contain the set $\boldsymbol{\Gamma}_\lambda$ tightly, to

approximate the feasible set. In other word, the aim of the current work is to find out a closed interval vector that contains all possible eigenvalues $\lambda_i, i = 1, 2, \ldots, n$, namely

$$\lambda_{ir} \in \lambda_{ir}^l = [\underline{\lambda}_{ir}, \bar{\lambda}_{ir}], \qquad \lambda_{im} \in \lambda_{im}^l = [\underline{\lambda}_{im}, \bar{\lambda}_{im}],$$
$$i = 1, 2, \ldots, n \tag{31}$$

where

$$\underline{\lambda}_{ir} = \min_{\mathbf{A}_{as} \in \mathbf{A}_{as}^l}\left\{\mathrm{Re}\left(\lambda_i(\mathbf{A}_{as})\right)\right\},$$
$$\bar{\lambda}_{ir} = \max_{\mathbf{A}_{as} \in \mathbf{A}_{as}^l}\left\{\mathrm{Re}\left(\lambda_i(\mathbf{A}_{as})\right)\right\}, \quad i = 1, 2, \ldots, n$$
$$\underline{\lambda}_{im} = \min_{\mathbf{A}_{as} \in \mathbf{A}_{as}^l}\left\{\mathrm{Im}\left(\lambda_i(\mathbf{A}_{as})\right)\right\}, \tag{32}$$
$$\bar{\lambda}_{im} = \max_{\mathbf{A}_{as} \in \mathbf{A}_{as}^l}\left\{\mathrm{Im}\left(\lambda_i(\mathbf{A}_{as})\right)\right\}, \quad i = 1, 2, \ldots, n$$

However, it is still difficult to find the exact interval bounds of the eigenvalues described by Eq. (31). For simplicity, but without losing accuracy, the first-order interval matrix perturbation algorithm [39] is employed to evaluate the interval bounds of eigenvalues of the state matrix of the concerned aeroelastic system with interval parameters since deviation amplitudes of uncertainties are assumed to be small in the current context. Firstly, we consider the following standard eigenvalue problem when the uncertain parameters are taken as nominal values

$$\mathbf{A}_{as}^c \boldsymbol{v}_i^c = \lambda_i^c \boldsymbol{v}_i^c, \quad i = 1, 2, \ldots, n \tag{33}$$

where $\boldsymbol{v}_i^c$ is the ith nominal right eigenvector corresponding to the ith nominal eigenvalue λ_i^c of $\mathbf{A}_{as}^c$. For convenience, we assume that the eigenvalues are distinct and the right eigenvectors are biorthonormal which have been normalized so as to satisfy

$$\left(\boldsymbol{v}_j^c\right)^T \boldsymbol{v}_i^c = \delta_{ij}, \quad i, j = 1, 2, \ldots, n \tag{34}$$

where δ_{ij} is the Kronecker delta symbol. Then, we give a small perturbation $\delta\mathbf{A}_{as} \in \mathbf{A}_{as}^l$ to the nominal state matrix $\mathbf{A}_{as}^c$, and the perturbed form of the standard eigenvalue problem can be obtained as follows

$$\left(\mathbf{A}_{as}^c + \delta\mathbf{A}_{as}\right)\left(\boldsymbol{v}_i^c + \delta\boldsymbol{v}_i\right) = \left(\lambda_i^c + \delta\lambda_i\right)\left(\boldsymbol{v}_i^c + \delta\boldsymbol{v}_i\right),$$
$$i = 1, 2, \ldots, n \tag{35}$$

where $\delta\lambda_i$ and $\delta\boldsymbol{v}_i$ are the ith first-order perturbation eigenvalue and eigenvector, respectively. Expanding Eq. (35) and ignoring the second-order terms, we have

$$\mathbf{A}_{as}^c \boldsymbol{v}_i^c + \mathbf{A}_{as}^c \delta\boldsymbol{v}_i + \delta\mathbf{A}_{as}\boldsymbol{v}_i^c = \lambda_i^c \boldsymbol{v}_i^c + \lambda_i^c\delta\boldsymbol{v}_i + \delta\lambda_i\boldsymbol{v}_i^c,$$
$$i = 1, 2, \ldots, n \tag{36}$$

Recalling the first formula in Eq. (33), Eq. (36) can be rewritten as follows

$$\mathbf{A}_{as}^c \delta\boldsymbol{v}_i + \delta\mathbf{A}_{as}\boldsymbol{v}_i^c = \lambda_i^c\delta\boldsymbol{v}_i + \delta\lambda_i\boldsymbol{v}_i^c, \quad i = 1, 2, \ldots, n \tag{37}$$

Here, we assume that the perturbation eigenvectors can be expressed as a linear combination of nominal right eigenvectors and have the expression [40]

$$\delta\boldsymbol{v}_i = \sum_{j=1}^n \varepsilon_{ij}\boldsymbol{v}_j^c, \quad \varepsilon_{ii} = 0, \quad i = 1, 2, \ldots, n \tag{38}$$

where $\varepsilon_{ij}(i \neq j)$ are small coefficients. Premultiplying both sides of Eq. (37) by $\left(\boldsymbol{v}_i^c\right)^T$ yields

$$\left(\boldsymbol{v}_i^c\right)^T\mathbf{A}_{as}^c\delta\boldsymbol{v}_i + \left(\boldsymbol{v}_i^c\right)^T\delta\mathbf{A}_{as}\boldsymbol{v}_i^c = \left(\boldsymbol{v}_i^c\right)^T\lambda_i^c\delta\boldsymbol{v}_i + \left(\boldsymbol{v}_i^c\right)^T\delta\lambda_i\boldsymbol{v}_i^c,$$
$$i = 1, 2, \ldots, n \tag{39}$$

Considering the normalized and biorthonormal condition of right eigenvectors, we have

$$
\left(\boldsymbol{v}_i^c\right)^T \mathbf{A}_{as}^c \delta \boldsymbol{v}_i = \left(\boldsymbol{v}_i^c\right)^T \mathbf{A}_{as}^c \sum_{j=1}^n \varepsilon_{ij} \boldsymbol{v}_j^c = \sum_{j=1}^n \varepsilon_{ij} \left(\boldsymbol{v}_i^c\right)^T \lambda_j^c \boldsymbol{v}_j^c
$$
$$
= \sum_{j=1}^n \varepsilon_{ij} \lambda_j^c \delta_{ij} = \mathbf{0}
\tag{40}
$$
$$
\left(\boldsymbol{v}_i^c\right)^T \lambda_i^c \delta \boldsymbol{v}_i = \left(\boldsymbol{v}_i^c\right)^T \lambda_i^c \sum_{j=1}^n \varepsilon_{ij} \boldsymbol{v}_j^c = \sum_{j=1}^n \varepsilon_{ij} \lambda_i^c \delta_{ij} = \mathbf{0},
$$
$$
\left(\boldsymbol{v}_i^c\right)^T \delta \lambda_i \boldsymbol{v}_i^c = \delta \lambda_i, \quad i = 1, 2, \ldots, n
$$

Thus, the first-order perturbed eigenvalues with respect to the perturbed state matrix $\mathbf{A}_{as} = \mathbf{A}_{as}^c + \delta \mathbf{A}_{as}$ can be obtained as follow

$$
\lambda_i = \lambda_i^c + \delta \lambda_i = \lambda_i^c + \left(\boldsymbol{v}_i^c\right)^T \delta \mathbf{A}_{as} \boldsymbol{v}_i^c, \quad i = 1, 2, \ldots, n
\tag{41}
$$

Since the eigenvalues are complex numbers, Eq. (41) can also be expressed in the real and imaginary part form as

$$
\lambda_i = \lambda_{ir} + \sqrt{-1}\lambda_{im} = \lambda_{ir}^c + \delta \lambda_{ir} + \sqrt{-1}\left(\lambda_{im}^c + \delta \lambda_{im}\right)
\tag{42}
$$

where λ_{ir} and λ_{im} are the real and imaginary parts of the eigenvalues, respectively, $\delta \lambda_{ir}$ and $\delta \lambda_{im}$ are the corresponding perturbation terms. Combining Eq. (42) and Eq. (41) and introducing the real and imaginary part form of the eigenvectors yield the following expression

$$
\left(\boldsymbol{v}_{ir}^c + \sqrt{-1}\boldsymbol{v}_{im}^c\right)^T \delta \mathbf{A}_{as} \left(\boldsymbol{v}_{ir}^c + \sqrt{-1}\boldsymbol{v}_{im}^c\right) = \delta \lambda_{ir} + \sqrt{-1}\delta \lambda_{im}
\tag{43}
$$

Expanding Eq. (43) and respectively considering the real part and the imaginary parts yield

$$
\delta \lambda_{ir}^c = \left(\boldsymbol{v}_{ir}^c\right)^T \delta \mathbf{A}_{as} \boldsymbol{v}_{ir}^c - \left(\boldsymbol{v}_{im}^c\right)^T \delta \mathbf{A}_{as} \boldsymbol{v}_{im}^c
$$
$$
\delta \lambda_{im}^c = \left(\boldsymbol{v}_{ir}^c\right)^T \delta \mathbf{A}_{as} \boldsymbol{v}_{im}^c + \left(\boldsymbol{v}_{im}^c\right)^T \delta \mathbf{A}_{as} \boldsymbol{v}_{ir}^c
\tag{44}
$$

With the help of interval mathematics, we can obtain the following interval extension of the real part of complex eigenvalues from Eq. (42) and Eq. (44)

$$
\lambda_{ir}^I = \lambda_{ir}^c + \Delta \lambda_{ir}^I, \quad i = 1, 2, \ldots, n
\tag{45}
$$

where $\Delta \lambda_{ir}^I = [-\Delta \lambda_{ir}, \Delta \lambda_{ir}] = \left(\boldsymbol{v}_{ir}^c\right)^T \Delta \mathbf{A}_{as}^I \boldsymbol{v}_{ir}^c - \left(\boldsymbol{v}_{im}^c\right)^T \Delta \mathbf{A}_{as}^I \boldsymbol{v}_{im}^c$ and $\Delta \lambda_{ir}$ are the radiuses of the real parts of complex eigenvalues. Then, by using the interval operation algorithm, the interval bounds of the real parts of complex eigenvalues can be achieved as

$$
\lambda_{ir}^I = [\underline{\lambda}_{ir}, \bar{\lambda}_{ir}] = \left[\lambda_{ir}^c - \Delta \lambda_{ir}, \lambda_{ir}^c + \Delta \lambda_{ir}\right], \quad i = 1, 2, \ldots, n
\tag{46}
$$

where $\Delta \lambda_{ir} = |\boldsymbol{v}_{ir}^c|^T \Delta \mathbf{A}_{as} |\boldsymbol{v}_{ir}^c| + |\boldsymbol{v}_{im}^c|^T \Delta \mathbf{A}_{as} |\boldsymbol{v}_{im}^c|$.

Similarly, the interval bounds of the imaginary parts of complex eigenvalues can also be obtained as follows by using the operations discussed above

$$
\lambda_{im}^I = [\underline{\lambda}_{im}, \bar{\lambda}_{im}] = \left[\lambda_{im}^c - \Delta \lambda_{im}, \lambda_{im}^c + \Delta \lambda_{im}\right], \quad i = 1, 2, \ldots, n
\tag{47}
$$

where $\Delta \lambda_{im} = |\boldsymbol{v}_{ir}^c|^T \Delta \mathbf{A}_{as} |\boldsymbol{v}_{im}^c| + |\boldsymbol{v}_{im}^c|^T \Delta \mathbf{A}_{as} |\boldsymbol{v}_{ir}^c|$.

Finally, we can obtain the following interval estimation of eigenvalues of the interval state matrix $\mathbf{A}_{as}^I$ through Eq. (46) and Eq. (47)

$$
\lambda_i^I = \lambda_{ir}^I + \sqrt{-1}\lambda_{im}^I, \quad i = 1, 2, \ldots, n
\tag{48}
$$

Once the lower and upper bounds of eigenvalues of the interval state matrix of the aeroelastic state-space model are find out based

on the first-order interval matrix perturbation algorithm proposed above, the stability of the investigated aeroelastic system with interval uncertainties can be evaluated according to the stability criterion used for uncertain circumstances defined at the beginning of this subsection. To simplify representation, we can redefine the equivalent stability norm for the interval state matrix $\mathbf{A}_{as}^I$ of the uncertain aeroelastic state-space model with the premise of a given dynamic pressure q, namely, $\mathbf{A}_{as}^I$ is robustly stable, possibly stable and absolutely unstable when $\max_{i=1,2,\ldots,n}\{\bar{\lambda}_{ir}(\mathbf{A}_{as}^I(q))\} < 0$, $\max_{i=1,2,\ldots,n}\{\underline{\lambda}_{ir}(\mathbf{A}_{as}^I(q))\} < 0$ while $\max_{i=1,2,\ldots,n}\{\bar{\lambda}_{ir}(\mathbf{A}_{as}^I(q))\} \geq 0$ and $\max_{i=1,2,\ldots,n}\{\underline{\lambda}_{ir}(\mathbf{A}_{as}^I(q))\} \geq 0$, respectively.

Obviously, the lower and upper bounds of eigenvalues of the concerned interval state matrix is changing with the dynamic pressure q of the freestream. Hence, by changing the dynamic pressure, we can obtain a banded root locus of the uncertain aeroelastic system on the complex plane and determine the critical dynamic pressure $\underline{q}^*$ and $\bar{q}^*$ corresponding to the interval aeroelastic state matrix converting from robust stability to possible stability and from possible stability to absolute instability respectively, which satisfy

$$
\max_{i=1,2,\ldots,n}\left\{\bar{\lambda}_{ir}\left(\mathbf{A}_{as}^I(\underline{q}^*)\right)\right\} = 0 \quad \text{and}
$$
$$
\max_{i=1,2,\ldots,n}\left\{\underline{\lambda}_{ir}\left(\mathbf{A}_{as}^I(\bar{q}^*)\right)\right\} = 0
\tag{49}
$$

In general, the critical dynamic pressure $\underline{q}^*$ and $\bar{q}^*$ can be equivalently converted to the lower and upper bounds of the flutter speed index $\underline{V}_f^*$ and $\bar{V}_f^*$ respectively, which are crucial dimensionless design parameters in the aeroelastic design of aircrafts.

Now, by means of the proposed stability analysis method, the robust flutter boundary of the aeroelastic state-space model constructed based on the aerodynamic ROM in presence of interval uncertainties can be conveniently predicted, and the flowchart is concisely illustrated in Fig. 1. In contrast to the deterministic aeroelastic system, the root locus of the interval state matrix of the uncertain aeroelastic system associated with different dynamic pressures is transformed from a simple curve into a banded region with a certain width, and the critical dynamic pressure and flutter speed index become interval numbers instead of deterministic numbers as well. Moreover, due to the impact of uncertainties, the state of the aeroelastic system of interest is divided into three types, namely robust stability, possible stability and absolute instability, by the lower and upper bounds of the flutter speed index. In practical engineering, both the situations of possible stability and absolute instability are not permitted in order to guarantee the safety of the aircraft structure. Hence, the lower bound of the flutter velocity is a greater concern to engineers compared to the upper bound.

4. Numerical examples

In this section, we apply the proposed method to the uncertain aerodynamic ROM constructions and robust flutter boundary predictions of the two-dimensional Isogai wing and three-dimensional AGARD 445.6 wing. Computational results are compared with those obtained by MCS as well as other numerical or experimental methods to assess the validity and accuracy of the developed algorithm.

4.1. Example I: Isogai wing

In this example, the two-dimensional Isogai wing model [41, 42], a numerical benchmark case for aeroelastic analysis, is selected to validate the proposed method as shown in Fig. 2. This model has two degrees of freedom of plunging and pitching with a NACA 64A010 airfoil section. The structural parameters chosen
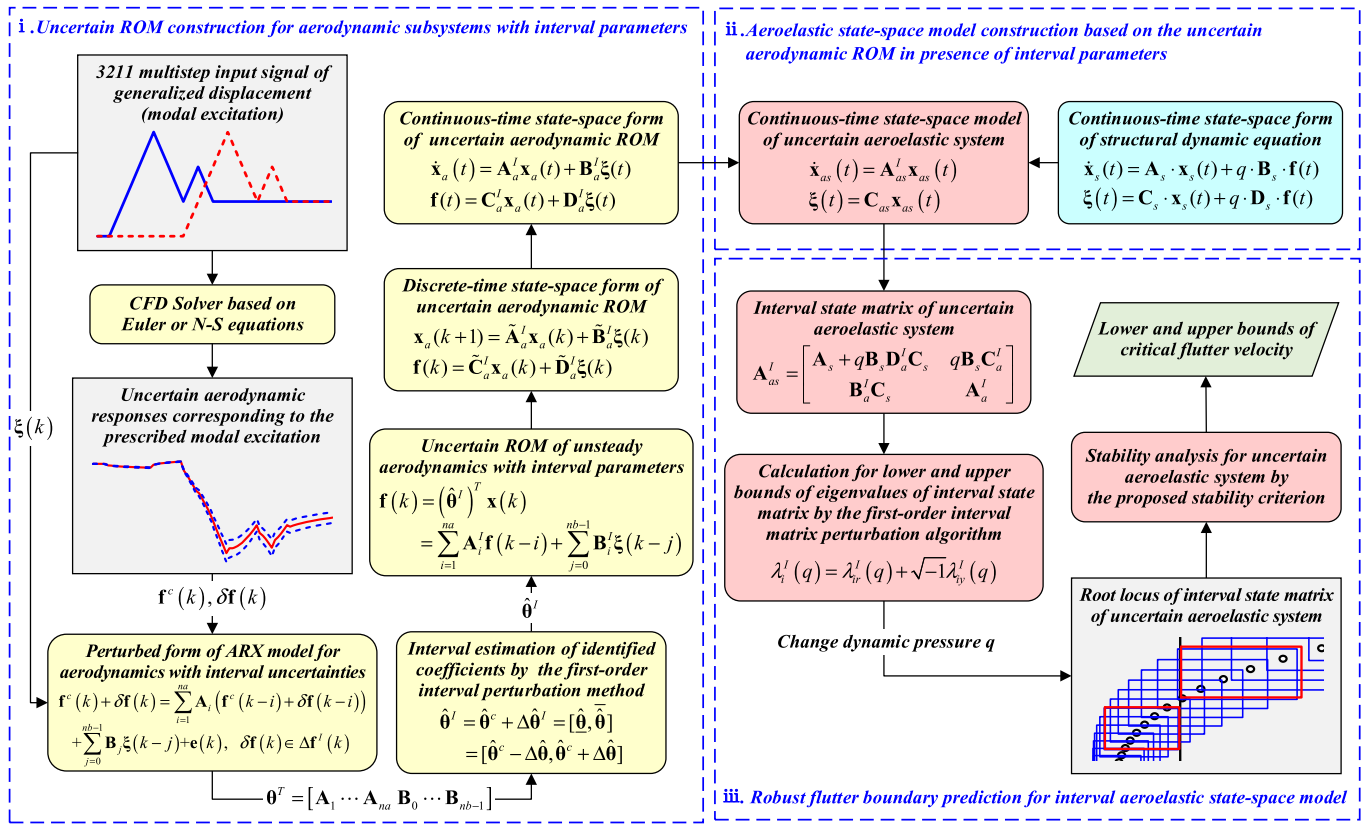
i . *Uncertain ROM construction for aerodynamic subsystems with interval parameters*

3211 multistep input signal of generalized displacement (modal excitation)

CFD Solver based on Euler or N-S equations

Uncertain aerodynamic responses corresponding to the prescribed modal excitation

$\mathbf{f}^c(k), \delta\mathbf{f}(k)$

Perturbed form of ARX model for aerodynamics with interval uncertainties
$$\mathbf{f}^c(k) + \delta\mathbf{f}(k) = \sum_{i=1}^{na} \mathbf{A}_i \left(\mathbf{f}^c(k-i) + \delta\mathbf{f}(k-i) \right)$$
$$+ \sum_{j=0}^{nb-1} \mathbf{B}_j \xi(k-j) + \mathbf{e}(k), \quad \delta\mathbf{f}(k) \in \Delta\mathbf{f}^I(k)$$

$\xi(k)$

$$\boldsymbol{\theta}^T = \begin{bmatrix} \mathbf{A}_1 \cdots \mathbf{A}_{na} \ \mathbf{B}_0 \cdots \mathbf{B}_{nb-1} \end{bmatrix}$$

Continuous-time state-space form of uncertain aerodynamic ROM
$$\dot{\mathbf{x}}_a(t) = \mathbf{A}_a^I \mathbf{x}_a(t) + \mathbf{B}_a^I \xi(t)$$
$$\mathbf{f}(t) = \mathbf{C}_a^I \mathbf{x}_a(t) + \mathbf{D}_a^I \xi(t)$$

Discrete-time state-space form of uncertain aerodynamic ROM
$$\mathbf{x}_a(k+1) = \tilde{\mathbf{A}}_a^I \mathbf{x}_a(k) + \tilde{\mathbf{B}}_a^I \xi(k)$$
$$\mathbf{f}(k) = \tilde{\mathbf{C}}_a^I \mathbf{x}_a(k) + \tilde{\mathbf{D}}_a^I \xi(k)$$

Uncertain ROM of unsteady aerodynamics with interval parameters
$$\mathbf{f}(k) = \left(\hat{\boldsymbol{\theta}}^I \right)^T \mathbf{x}(k)$$
$$= \sum_{i=1}^{na} \mathbf{A}_i^I \mathbf{f}(k-i) + \sum_{j=0}^{nb-1} \mathbf{B}_i^I \xi(k-j)$$

$\hat{\boldsymbol{\theta}}^I$

Interval estimation of identified coefficients by the first-order interval perturbation method
$$\hat{\boldsymbol{\theta}}^I = \hat{\boldsymbol{\theta}}^c + \Delta\hat{\boldsymbol{\theta}}^I = [\hat{\underline{\boldsymbol{\theta}}}, \overline{\hat{\boldsymbol{\theta}}}]$$
$$= [\hat{\boldsymbol{\theta}}^c - \Delta\hat{\boldsymbol{\theta}}, \hat{\boldsymbol{\theta}}^c + \Delta\hat{\boldsymbol{\theta}}]$$

ii . *Aeroelastic state-space model construction based on the uncertain aerodynamic ROM in presence of interval parameters*

Continuous-time state-space model of uncertain aeroelastic system
$$\dot{\mathbf{x}}_{as}(t) = \mathbf{A}_{as}^I \mathbf{x}_{as}(t)$$
$$\xi(t) = \mathbf{C}_{as} \mathbf{x}_{as}(t)$$

Continuous-time state-space form of structural dynamic equation
$$\dot{\mathbf{x}}_s(t) = \mathbf{A}_s \cdot \mathbf{x}_s(t) + q \cdot \mathbf{B}_s \cdot \mathbf{f}(t)$$
$$\xi(t) = \mathbf{C}_s \cdot \mathbf{x}_s(t) + q \cdot \mathbf{D}_s \cdot \mathbf{f}(t)$$

Interval state matrix of uncertain aeroelastic system
$$\mathbf{A}_{as}^I = \begin{bmatrix} \mathbf{A}_s + q\mathbf{B}_s\mathbf{D}_a^I\mathbf{C}_s & q\mathbf{B}_s\mathbf{C}_a^I \\ \mathbf{B}_a^I\mathbf{C}_s & \mathbf{A}_a^I \end{bmatrix}$$

Calculation for lower and upper bounds of eigenvalues of interval state matrix by the first-order interval matrix perturbation algorithm
$$\lambda_i^I(q) = \lambda_{ir}^I(q) + \sqrt{-1}\lambda_{iy}^I(q)$$

Change dynamic pressure q

Lower and upper bounds of critical flutter velocity

Stability analysis for uncertain aeroelastic system by the proposed stability criterion

Root locus of interval state matrix of uncertain aeroelastic system

iii . *Robust flutter boundary prediction for interval aeroelastic state-space model*

Fig. 1. Flowchart of robust flutter analysis based on the uncertain aerodynamic ROM with interval parameters.

Fig. 2. Isogai wing with two degrees of freedom.

for this model are $x_\alpha = 1.8$, $r_\alpha^2 = 3.48$, $a = -2.0$, $\omega_h = 100$ rad/s, $\omega_\alpha = 100$ rad/s, and $\mu = 60$, where x_α is the dimensionless distance of center of gravity behind stiffness center, r_α denotes the dimensionless gyration radius of the airfoil around stiffness center, a stands for the dimensionless distance of elastic axis behind midchord, ω_h and ω_α are the uncoupled natural frequencies of airfoil in plunge and pitch respectively, and μ is the mass ratio. These parameters were empirically chosen by Isogai in order to simulate the bending and torsion motions of an outboard section of a sweptback wing.

For the current example, the thickness of innermost layer of the body-fitted grid, the circumferential grid sizes of the airfoil and the outflow boundary condition of the flow field are chosen as uncertain sources that may affect the aerodynamic responses in CFD simulation. As shown in Fig. 3, the flow field of the model is discretized using structured grids. The thicknesses of the innermost layers of the body-fitted grids are set at three levels, respectively, as 1×10^{-5} m, 5×10^{-5} m and 1×10^{-4} m. The three levels of circumferential grid numbers of the airfoil are 150, 200 and 250. The pressure far field and pressure outlet are treated as two types

of outflow boundary conditions of the flow field. By the free combination of the aforementioned mesh scales and boundary conditions, we can obtain 18 flow field modeling schemes in total, all that are frequently used in aerodynamic numerical simulation.

For the two-dimensional aeroelastic model in this example, we consider the transonic freestream condition $Ma = 0.825$ at zero mean angle of attack and all of the calculations are in the dimensionless form. Here, the "3211" multistep input signals of plunging and pitching displacements as illustrated in Fig. 4 are used as the modal excitations. An inviscid Euler equation-based unsteady CFD solver has the ability to simulate the transonic flow with shock waves, which will be used for unsteady flow computations during the training of the aerodynamic ROM in the numerical examples in this paper. The spatial discretization is accomplished by the first order upwind scheme while the physical time discretization is implemented by the second order implicit scheme. The dimensionless time step size used for the training of the aerodynamic ROM in the current example is $\Delta\tau = 0.3$. Based on the foregoing 18 kinds of flow field modeling schemes, a series of unsteady generalized aerodynamic responses of the investigated model corresponding to the prescribed modal excitations are extracted from the CFD solver. The CFD-induced uncertainty of the obtained aerodynamic responses are quantified as interval numbers by use of the non-probabilistic quantification method proposed by Wang et al. [43]. The central values of the quantified intervals are treated as nominal aerodynamic responses and the percentage radii of the interval responses corresponding to the prescribed modal excitations are demonstrated in Fig. 5. Among these percentage radii, the maximum values are used as percentage estimations of interval radii of the CFD-based generalized aerodynamic responses.

Then, the estimated interval generalized aerodynamic responses and the prescribed modal excitations are fed into Eq. (2) to construct the ROM-UAR for approximating the uncertain aerodynamic subsystem of the Isogai wing in transonic regime while the con-
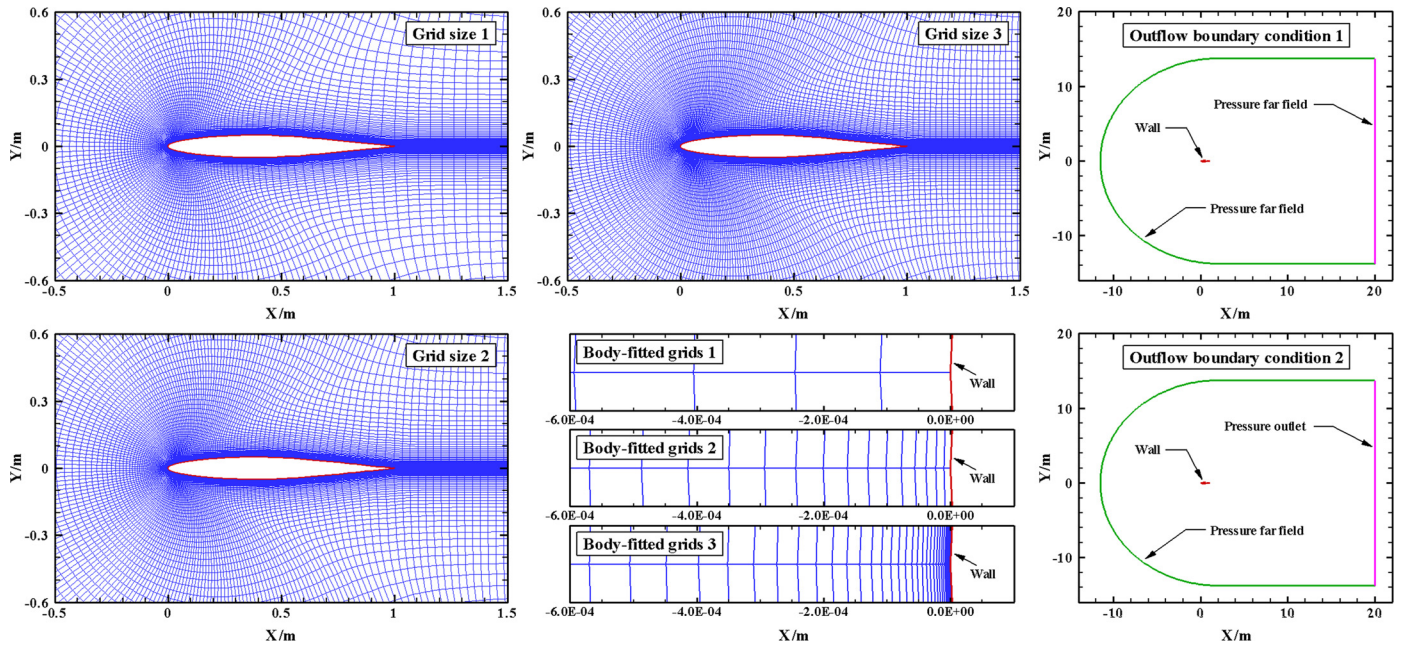
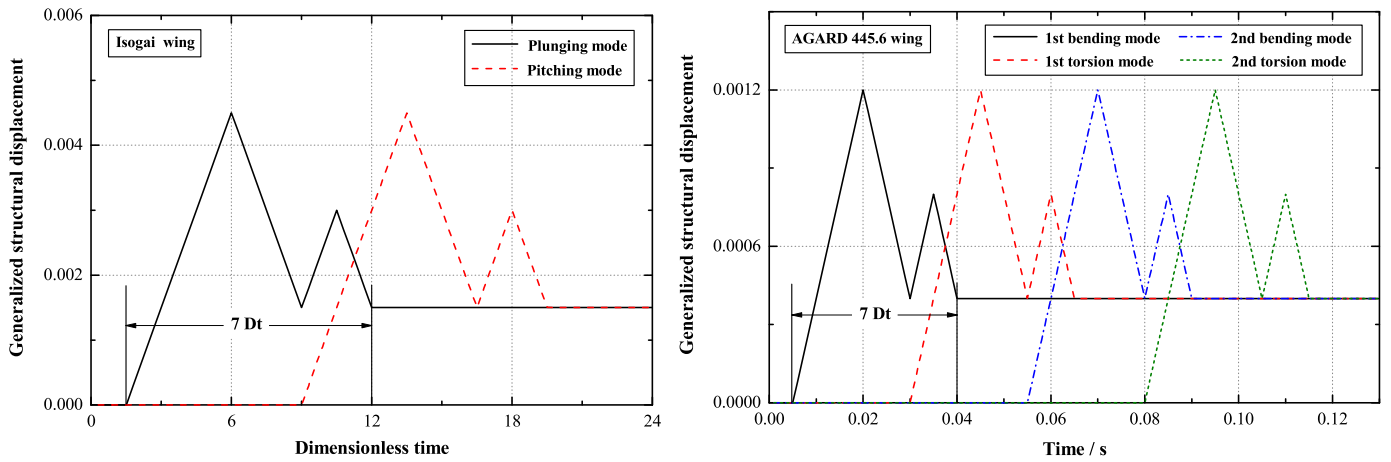**Fig. 3.** Different levels and types of mesh scales and outflow boundary conditions.

Fig. 4. Designed 3211 multistep input signal of generalized displacements (modal excitations).
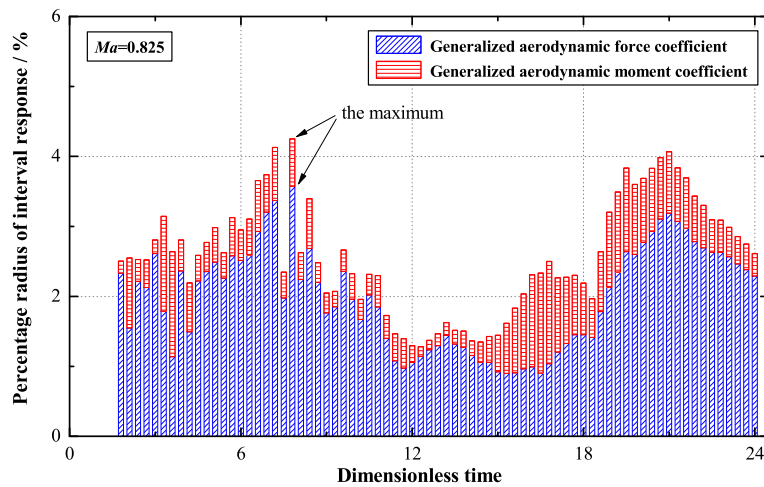

Fig. 5. The percentage radii of intervals of generalized aerodynamic coefficients generated by the CFD solver.
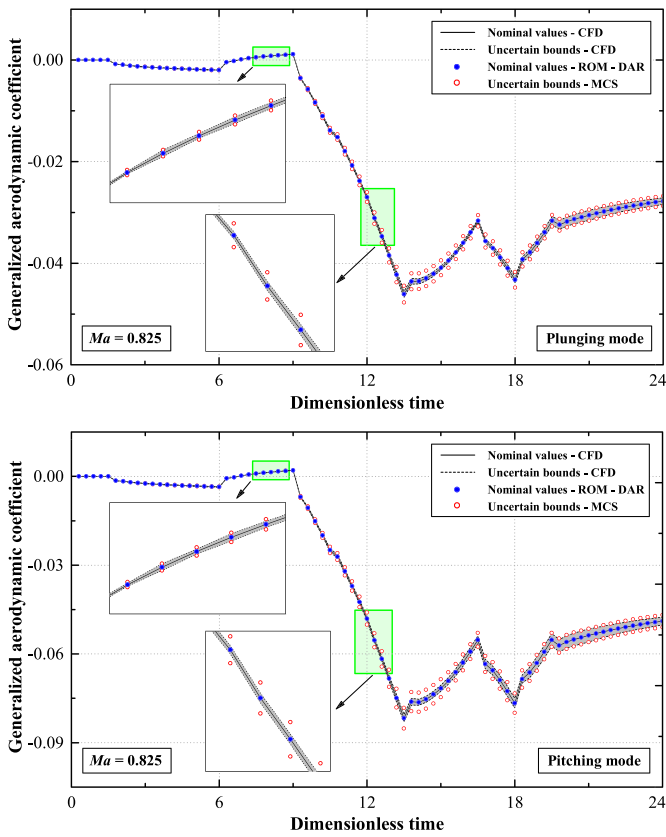
Fig. 6. Uncertain aerodynamic responses at $Ma = 0.825$ corresponding to the modal excitations presented in Fig. 4.

ventional ROM-DAR is used to represent the deterministic aerodynamic subsystem with nominal aerodynamic responses. As a comparison, the MCS is conducted where the uncertain generalized aerodynamic coefficients are assumed to satisfy a uniform distribution within the estimated interval bounds. Here, we use 5000 groups of generalized aerodynamic coefficients, which are generated randomly from the interval uncertain space, to construct a series of ROMs-DAR. The delay orders of outputs and inputs of the above ROM-DAR and ROM-UAR are taken as $na = 4$ and $nb = 4$, respectively, since the error of the ROM with the current orders

is proved to be relatively small compared with that using other possible delay orders for this example. As shown in Fig. 6, the nominal values of generalized aerodynamic responses calculated by the ROM-DAR agree quite well with those directly produced by the CFD solver. It also can be seen from Fig. 6 that the interval range of the uncertain aerodynamic responses determined through MCS are slightly wider than those of the original CFD-generated aerodynamic responses due to a little over estimation of uncertainties of primary CFD responses. Besides, the interval bounds of uncertain aerodynamic responses obtained by MCS absolutely contain the counterparts of CFD results. These results indicate that the MCS can provide a reasonably accurate prediction for the uncertain aerodynamic responses corresponding to the prescribed modal excitations and can be used as reference for the method developed in this paper. The lower and upper bounds of identified coefficients involved in the ROM-UAR estimated by Eq. (16) are almost consistent with those determined via MCS and completely contain the identified coefficients of the nominal aerodynamic ROM as demonstrated in Fig. 7, in which LB, UB and NV are the abbreviations of lower bound, upper bound and nominal value, respectively. Qualitatively, we can conclude that the proposed ROM-UAR can be employed to replace the CFD solver for the uncertain response calculation of a two-dimensional aerodynamic subsystem where CFD-induced uncertainties are considered.

The constructed ROM-UAR is coupled with the dimensionless structural dynamic equation without damping formulated in the modal basis coordinates to generate the uncertain aeroelastic system of the Isogai wing. With the help of Eq. (46) and Eq. (47), we can estimate the lower and upper bounds of eigenvalues of the interval state matrix of the uncertain aeroelastic system at a specified dynamic pressure of the freestream. Fig. 8 gives the loci of interval bounds of eigenvalues for the uncertain aeroelastic system as well as the loci of eigenvalues for the nominal aeroelastic system associated with dynamic pressures. As indicated in Fig. 8, the flutter of the wing is caused by the first mode for this particular condition. A detail view of the first root loci of the wing traversing the real axis of the complex plane is illustrated in Fig. 9. The interval bounds of the first root loci of the uncertain aeroelastic system calculated by the proposed method are also compared with counterparts obtained by MCS in Fig. 9. Here, the results of MCS gained via repetitive deterministic aeroelastic analyses based on the conventional ROM-DAR for each sample are considered to be exact. Different from the deterministic circum-
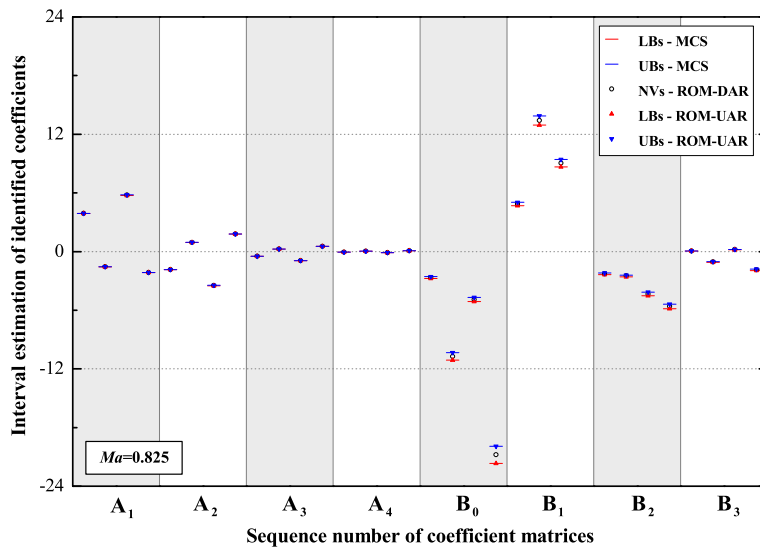

Fig. 7. Comparison of interval estimations of identified coefficients involved in the reduced-order model of the uncertain aerodynamic subsystem calculated by ROM-UAR with counterparts obtained by MCS at $Ma = 0.825$.
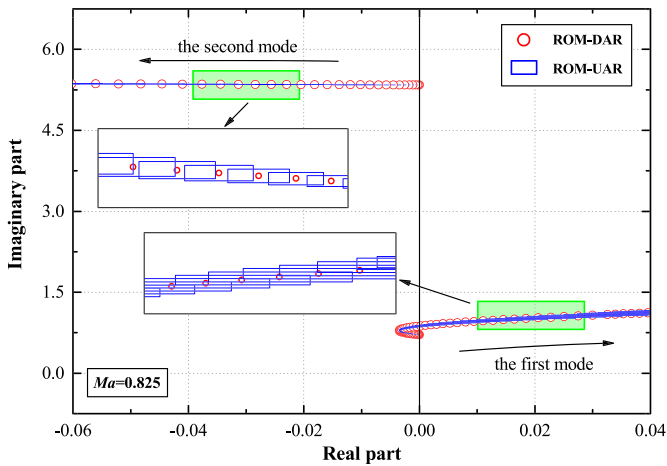
Fig. 8. Loci of interval bounds of eigenvalues for the Isogai wing varying with dynamic pressures at $Ma = 0.825$.
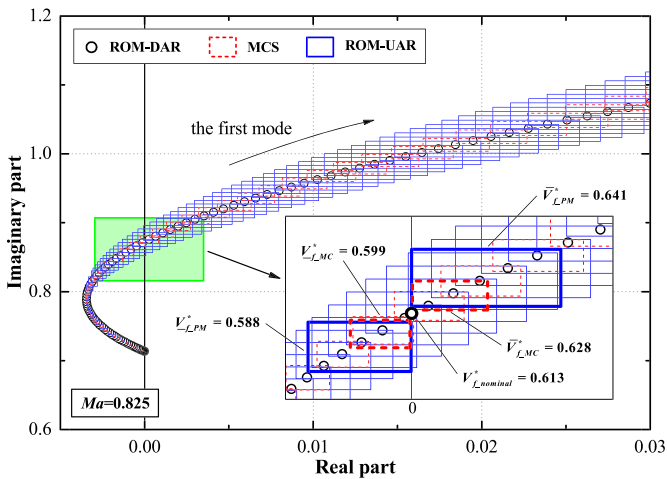

Fig. 9. Comparison of interval bounds of the first root loci for the Isogai wing calculated based on ROM-UAR with counterparts obtained by MCS at $Ma = 0.825$.
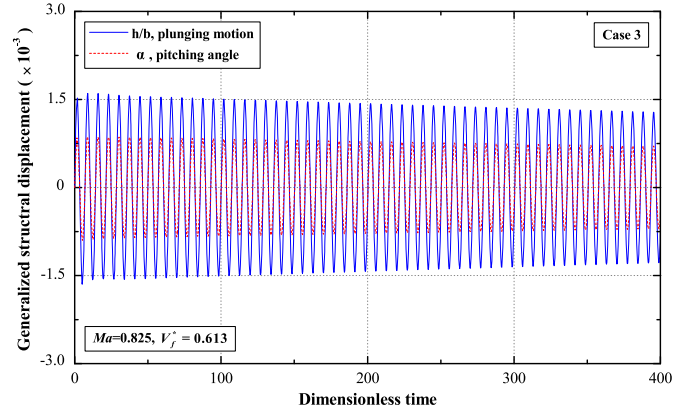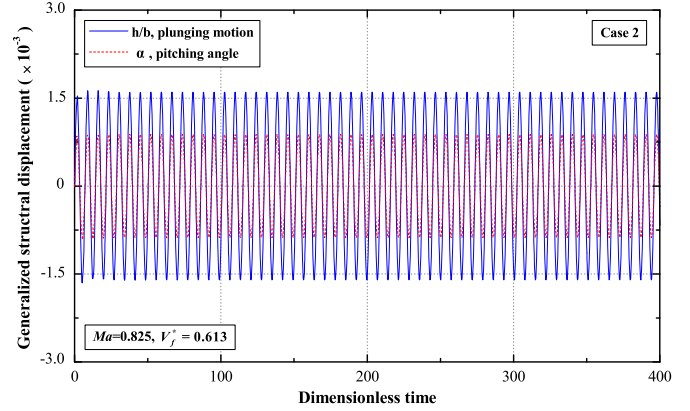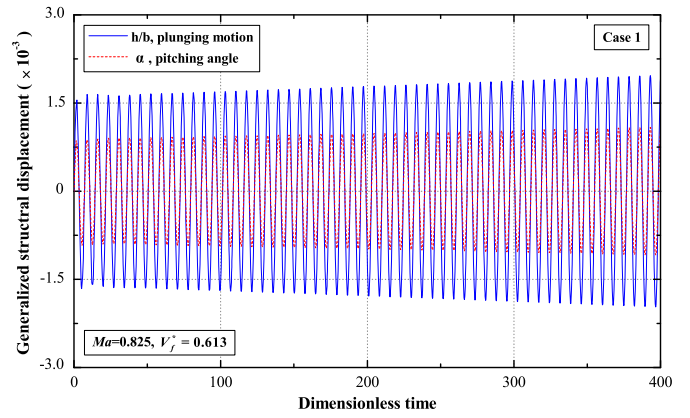

Fig. 10. Time history of generalized structural displacements for the Isogai wing at $Ma = 0.825$ and $V_f = 0.613$.

stance, the root locus of the uncertain aeroelastic system varying with dynamic pressures is transformed from a simple curve into a banded region consisting of a series of rectangular areas enclosed by the lower and upper bounds of the real and imaginary parts of eigenvalues. The lower and upper bounds of the flutter speed index are determined by using the robust stability criterion defined in subsection 3.2. The bounds of rectangular areas, in which the eigenvalues are distributed, corresponding to the lower and upper bounds of the flutter speed index calculated by the proposed method and MCS are highlighted in Fig. 9. In addition, Fig. 9 also indicates that the interval bounds of the root loci as well as the flutter speed index obtained through MSC are completely wrapped by those calculated by the proposed method due to the interval extension caused by interval operations. The proposed method can provide a reasonable prediction on the interval bounds of flutter speed index completely including the MCS bounds, the ROM-DAR-based nominal values and deterministic computational results in references [44] and [45] as compared in Table 1.

In order to reveal the impact of parametric uncertainty involved in the ROM-UAR caused by the aerodynamic uncertainty on the stability of the aeroelastic system, we execute aeroelastic time-marching simulations of the Isogai wing for three different cases at $Ma = 0.825$ and $V_f = 0.613$, which is equal to the nominal value of flutter speed index. The identified coefficients of the ROM-UAR are set as the obtained lower bounds in case 1, nominal values in case 2 and upper bounds in case 3. As shown in Fig. 10, both of the plunging and pitching amplitudes diverge, decay and remain constant over time for case 1, case 2 and case 3, indicat-
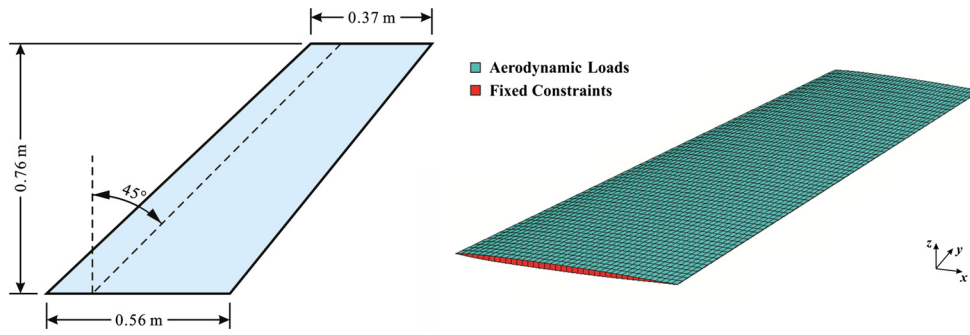
Table 1

Comparison of flutter speed index for the Isogai wing calculated in this paper with results in references at $Ma = 0.825$.

	NV-ROM-DAR	MCS-ROM-DAR		ROM-UAR		Alonso et al. (1994) [44]	Liu et al. (2001) [45]
		LB	UB	LB	UB		
Flutter speed index	0.613	0.599	0.628	0.588	0.641	0.612	0.630

Fig. 11. Planform view and structural FE model of the three-dimensional AGARD 445.6 wing.

Mode 1, Frequency=9.7055Hz

Mode 2, Frequency=37.7758Hz

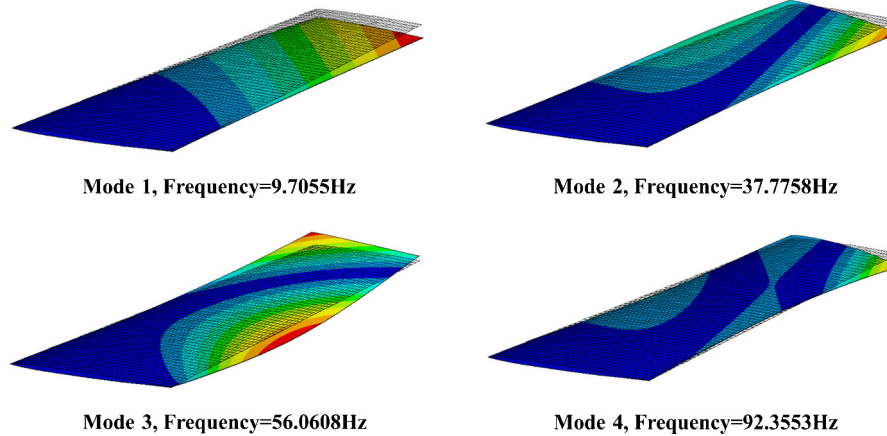Mode 3, Frequency=56.0608Hz

Mode 4, Frequency=92.3553Hz

Fig. 12. The first four modal shapes of the AGARD 445.6 wing.

ing that the aeroelastic systems are unstable, neutrally stable and stable, respectively. It means that due to aerodynamic uncertainty the aeroelastic system might be unstable under the nominal flutter speed. Therefore, the proposed approach can provide a more robust and more conservative prediction on flutter boundary than the conventional aeroelastic analysis method based on deterministic aerodynamic ROM.

Evidently, the uncertain parameters considered in this paper are far from covering all possible uncertainties involved in the aerodynamics. In addition to the above uncertain factors, the sources of aerodynamic uncertainties may also arise from simplifying assumptions, difference of convergence precision, errors of turbulence models if the viscosity is considered, different spatiotemporal discretization methods, unmodeled dynamics and so on. Hence, the uncertain factors chosen here are really a limited set of all possible uncertainties that influence the obtained aerodynamic response. In fact, the quantification of uncertainty sources is not the focus of this paper, and the interval bounds of the aerodynamics are only inputs of the proposed method. That is to say, the proposed method can be readily used to construct the uncertain aerodynamic ROM and predict the interval flutter boundaries as long as the interval information of the aerodynamics are quantified.

In addition, the time cost of a deterministic flutter speed prediction based on the full order model for the Isogai wing is about 1200 wall-clock hours run on a computer with a Intel i7-4790 3.60 GHz 8-core CPU and 16GB RAM. However, the time spent on the training of the aerodynamic ROM-DAR and the subsequent deterministic flutter speed prediction based on the obtained ROM-DAR are approximately 4 wall-clock hours and a few seconds, respectively, where the length of the input signal used in the current example is 80 dimensionless time steps. For the uncertain case, the time cost of quantifying the interval bounds of the generalized

aerodynamic coefficients is nearly 72 wall-clock hours. Once the interval bounds of the uncertain generalized aerodynamic coefficients are determined, it takes only a couple of seconds to obtain the lower and upper bounds of the flutter speed based on the proposed ROM-UAR, while the computational cost of predicting such interval bounds through the MCS is a few hours.

4.2. Example II: AGARD 445.6 wing

The AGARD 445.6 wing, a standard aeroelastic configuration, is used herein to verify the applicability of the proposed method in dealing with complex three-dimensional aeroelastic problems. Several different models of AGARD wing 445.6 were tested in the Transonic Dynamics Tunnel (TDT) at NASA Langley Research Center and the model designed as "Weakened 3" in reference [46] is investigated in the current example. A planform view of the AGARD 445.6 wing is shown in Fig. 11, which has a quarter-chord sweep angle of 45 degrees, an aspect ratio of 1.65, a taper ratio of 0.66, a wing semispan of 0.76 meters, a wing root chord of 0.56 meters, and a symmetric NACA 65A004 airfoil section. The wing employed is a semispan wind-tunnel-wall-mounted model constructed of laminated mahogany.

Anisotropic shell elements with variable thickness consistent with the airfoil section are adopted to generate the structural FE model as shown in Fig. 11. The material properties of the investigated model are as follows: $E_1 = 0.89$ GPa, $E_2 = 1.54$ GPa, $\nu = 0.31$, $G = 2.6$ GPa and $\rho = 381.98$ kg/m^3, in which E_1 denotes the Young's modulus in x-axial and z-axial direction, E_2 is the Young's modulus in y-axial direction, ν stands for the Poisson's ratio, G represents the shear modulus and ρ is the density of the model respectively. As shown in Fig. 12, the first four modal shapes of the model, namely first bending mode, first torsion mode, second bending mode and second torsion mode, are obtained by using

Table 2
Comparison of computed natural frequencies with measured and calculated values in references.

	Mode 1 / Hz	Mode 2 / Hz	Mode 3 / Hz	Mode 4 / Hz
Experimental data (Yates et al., 1963) [46]	9.60	38.10	50.70	98.50
Calculated values (Yates, 1987) [47]	9.60	38.17	48.35	91.54
Current paper	9.71	37.78	56.06	92.36

the structural mechanics solver. The computed natural frequencies ranging from 9.71 Hz for the first bending mode to 92.36 Hz for the second torsion mode in this paper match the experimental data and calculated counterparts in references [46] and [47] well as listed in Table 2. For the current example, the structural dynamic equation, in which no structural damping is considered, is formulated in the modal basis coordinates based on the first four modal shapes. The unsteady aerodynamic responses are generated by utilizing the inviscid Euler equation-based unsteady CFD solver where the flow field is discretized using unstructured/structured hybrid grids. The same as the first example, the spatial discretization is accomplished by the first order upwind scheme while the physical time discretization is implemented by the second order implicit scheme. The physical time step size used for the training of the aerodynamic ROM in this example is $\Delta t = 0.001$ s. The location and velocity of the fluid-solid coupling interface are updated by virtue of the dynamic mesh technique at each physical time step to match with the structural deformation of the wing induced by modal excitations.

We firstly consider the freestream condition $Ma = 0.901$ at zero angle of attack. The "3211" multistep input signals of first four generalized structural displacements as illustrated in Fig. 4 are still selected as the modal excitations. The first four generalized aerodynamic coefficients corresponding to the prescribed modal excitations in modal basis coordinates transformed from aerodynamic responses generated by the CFD solver in physical coordinates based on the modal shapes are considered to be nominal values. Here, we assume that the generalized aerodynamic coefficients obtained by the CFD solver have 5 percent uncertainties with regard to the nominal values and can be quantified by interval numbers. In this example, the proposed ROM-UAR is used to approximate the uncertain aerodynamic subsystem of the concerned AGARD 445.6 wing with interval aerodynamic responses while the conventional ROM-DAR is adopted to represent the deterministic aerodynamic subsystem with nominal aerodynamic responses. As a comparison, the MCS is conducted based on 5000 groups of generalized aerodynamic coefficients generated randomly from the assumed interval uncertain space, in which the uncertain generalized aerodynamic coefficients are assumed to satisfy a uniform distribution, to produce a series of ROMs-DAR. The delay orders of outputs and inputs of the ROM-DAR and ROM-UAR in the current example are also taken as $na = 4$ and $nb = 4$, respectively, after comparing the errors of ROMs with different possible orders. As shown in Fig. 13, the first four nominal generalized aerodynamic responses calculated by the ROM-DAR agree quite well with those directly produced by the CFD solver, and the interval bounds of uncertain aerodynamic responses determined through MCS match well with the assumed interval bounds of CFD-generated aerodynamic responses as well. Hence, the MCS results will be used as reference for the proposed method in the subsequent discussion. The lower and upper bounds of identified coefficients involved in the ROM-UAR estimated by the presented method are almost consistent with those determined via MCS and completely include the identified coefficients of the nominal aerodynamic ROM as demonstrated in Fig. 14. These results indicate that the proposed ROM-UAR can take the place of the CFD solver considering uncertainties in simulations to provide a reasonable

prediction of the uncertain aerodynamic responses of a three-dimensional wing.

The constructed ROM-UAR is coupled with the preceding structural dynamic equation to formulate the uncertain aeroelastic system of the AGARD 445.6 wing. Fig. 15 gives the loci of interval bounds of eigenvalues for the uncertain aeroelastic system as well as the loci of eigenvalues for the nominal aeroelastic system associated with dynamic pressures. It shows that the flutter branch of the uncertain aerodynamic elastic system is dominated by the first bending mode for the current condition. A detail view of the first root loci of the wing traversing the real axis of the complex plane is illustrated in Fig. 16. The interval bounds of the first root loci of the uncertain aeroelastic system calculated by the proposed method are also compared with counterparts obtained by MCS in Fig. 16. The lower and upper bounds of the flutter speed index calculated by the proposed method and MCS are highlighted in Fig. 16. We can obtain the same result as the first example that the interval bounds of the root loci as well as the flutter speed index obtained through MSC are completely wrapped by those calculated via the proposed method due to the interval extension induced by interval operations.

Using the aforementioned approach, we predict the robust flutter boundary of the AGARD 445.6 wing over the flight Mach number ranging from 0.499 to 1.141 experimentally measured by Yates et al. [46]. The calculated flutter characteristics are shown in Fig. 17, together with the experimental data, those obtained by MCS and other deterministic numerical methods. Qualitatively, the bounds of flutter speed index predicted by the developed robust flutter analysis method based on the ROM-UAR match well with the experimental values, MCS results and other deterministic computational results in the subsonic and transonic ranges. In the supersonic range, although a premature rise in the computational robust flutter boundary as compared with the experimental result is presented, Lee-Rausch et al. [48] and Zhang et al. [35] also over-predicted the flutter boundary by a similar amount compared to the central values of our interval results. In general, the proposed robust flutter analysis method can provide a reasonable prediction on the interval bounds of flutter speed index that includes the whole MCS bounds and nominal values determined based on the ROM-DAR as well as most of the experimental data and other deterministic numerical results. As illustrated in Fig. 17, the state of aeroelastic stability for the wing of interest is divided into three types, namely robust stability, possible stability and absolute instability, by the lower and upper bounds of the flutter speed index due to the influence of aerodynamic uncertainties. In terms of aeroelastic design, we should ensure the flight speed always in the robust stability region to avoid the occurrence of flutter. In this sense, the proposed approach may provide a more robust and conservative prediction on flutter boundary than the conventional aeroelastic analysis method based on deterministic aerodynamic ROM.

In terms of the computational efficiency, the time cost of a deterministic flutter speed prediction based on the full order model for the AGARD 445.6 wing is about 2280 wall-clock hours run on the same computer used in the first example. However, the time spent on the training of the aerodynamic ROM-DAR and the subsequent deterministic flutter speed prediction based on the obtained ROM-DAR are approximately 37 wall-clock hours and a few sec-
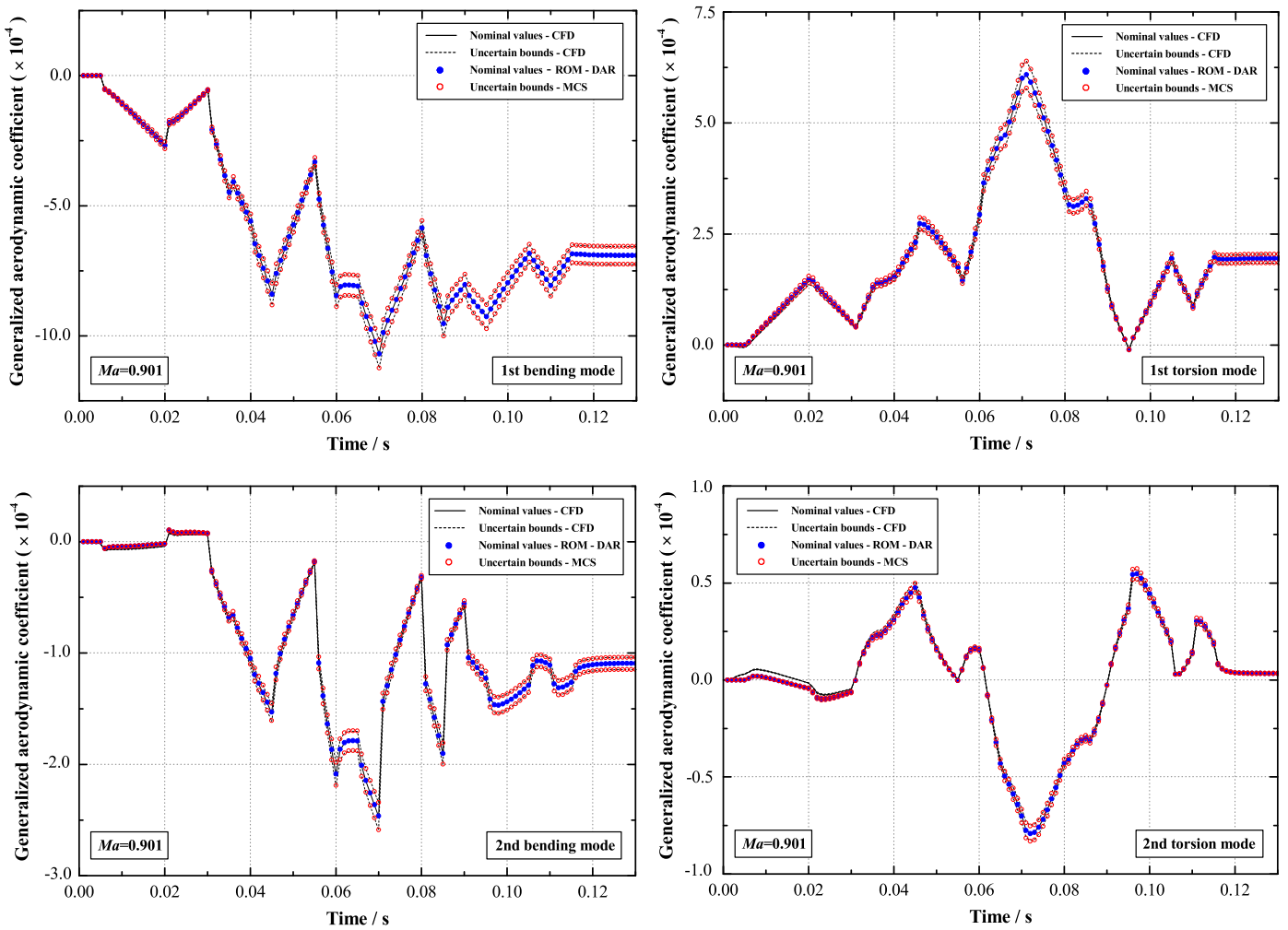
Fig. 13. Uncertain aerodynamic responses at $Ma = 0.901$ corresponding to the modal excitations presented in Fig. 4.
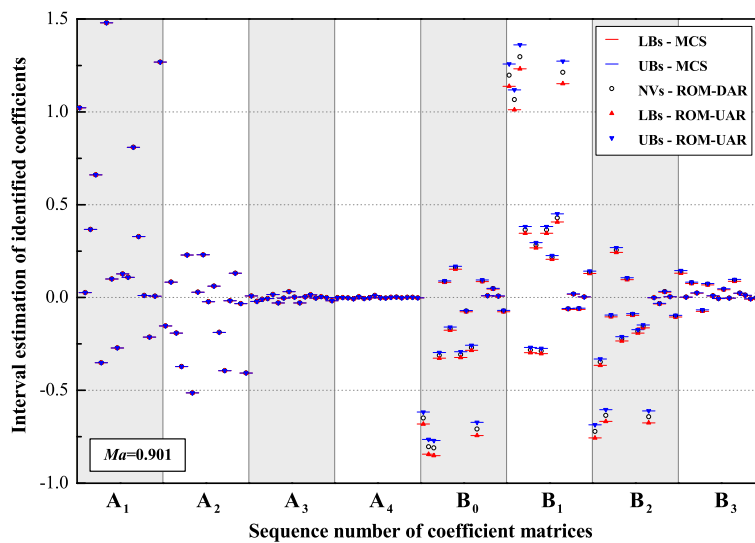

Fig. 14. Comparison of interval estimations of identified coefficients involved in the reduced-order model of the uncertain aerodynamic subsystem calculated by ROM-UAR with counterparts obtained by MCS at $Ma = 0.901$.

onds, respectively, where the length of the input signal used in this example is 130 physical time steps. Moreover, for an uncertain case, it still takes only a couple of seconds to obtain the lower and upper bounds of the flutter speed based on the pro-

posed ROM-UAR, while the computational cost of predicting such interval bounds through the MCS is a few hours once the interval bounds of the uncertain generalized aerodynamic coefficients are given. It is worth noting that quantifying the interval bounds
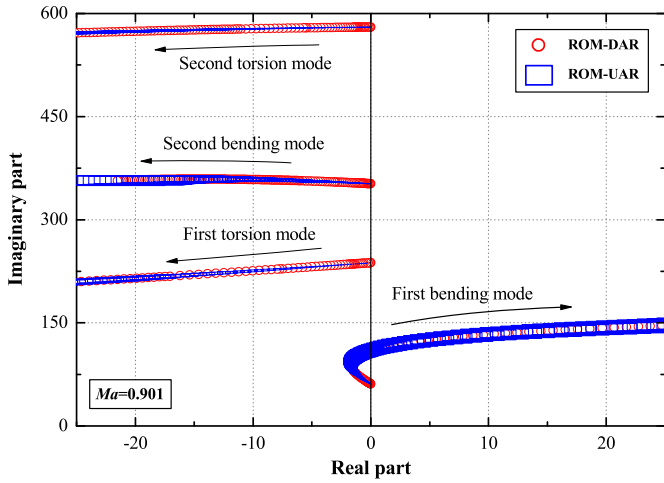
Fig. 15. Loci of interval bounds of eigenvalues for the AGARD 445.6 wing varying with dynamic pressures at $Ma = 0.901$.
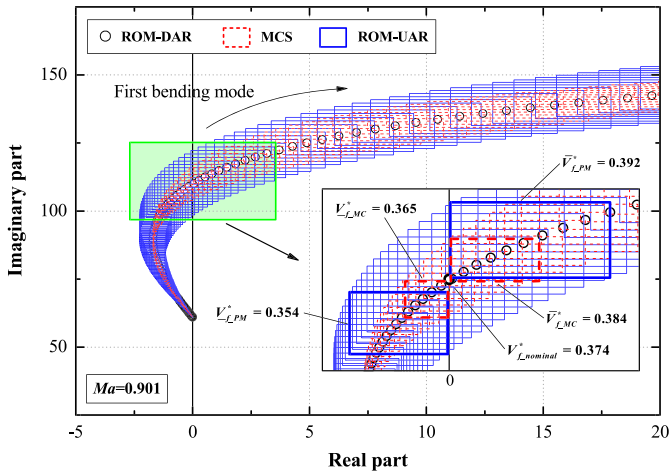
Fig. 16. Comparison of interval bounds of the first root loci for the AGARD 445.6 wing calculated by the proposed method with counterparts obtained by MCS at $Ma = 0.901$.

of the generalized aerodynamic coefficients are time consuming as well. The time cost of this process depends on the quantification method employed and is not considered in the evaluation of the computational efficiency of the proposed method.

5. Conclusion

This paper developed an uncertain CFD-based model reduction method for aerodynamic subsystems considering bounded uncertainties associated with CFD simulation with the help of the system identification theory and the interval perturbation approach. A new stability criterion for interval aeroelastic state matrices was defined to predict the robust flutter boundary of the concerned uncertain aeroelastic system based on the constructed uncertain aerodynamic ROM by using the standard interval eigenvalue solving algorithm. Synthesizing computational results of the aforementioned two numerical examples, some conclusions are summarized here:

1) The major characteristic of the proposed model reduction method is that the uncertain aerodynamic ROM, in which the coefficients are interval numbers instead of fixed numbers, obtained by this way is as uncertain as the original aerodynamic subsystem with CFD-induced uncertainties and can be used for aeroelastic uncertainty analysis.

2) Different from the deterministic circumstance, the root locus of the uncertain aeroelastic system associated with dynamic pressures is transformed from a simple curve into a banded region consisting of a series of rectangular areas enclosed by the lower and upper bounds of the real and imaginary parts of eigenvalues on the complex plane.

3) The state of stability for the aeroelastic system is divided into three types, namely robust stability, possible stability and absolute instability, by the lower and upper bounds of the flutter boundary due to the influence of aerodynamic uncertainties. In terms of aeroelastic design, the flight speed of the aeroelastic system must be kept in the robust stability region to avoid the occurrence of flutter.

In summary, by considering CFD-induced uncertainties, the proposed method can provide a more robust and conservative prediction on flutter boundary compared with the conventional aeroelastic analysis method based on the deterministic aerodynamic ROM. As a further research, the proposed model reduction method would be extended into the servo-aeroelasticity stability analysis, the active flutter suppression and the dynamic nonlinear aerodynamic model in the future work.

Conflict of interest statement
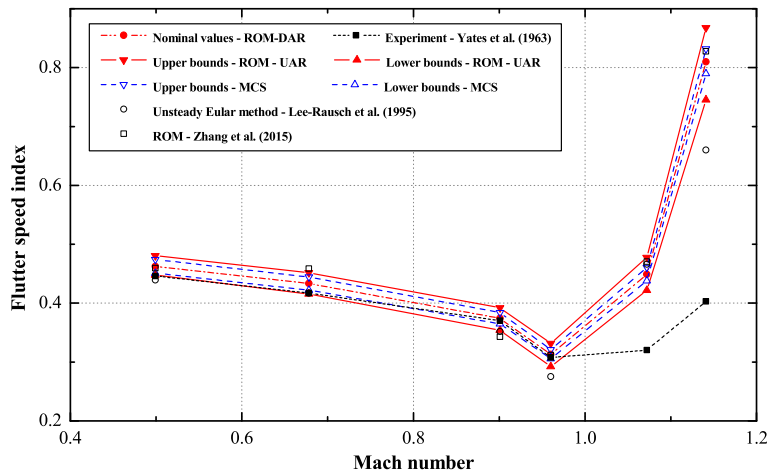
There is no conflict of interest.

Fig. 17. Comparison of flutter boundary predictions for the AGARD 445.6 wing obtained by the proposed method with those attained by other numerical or experimental methods.

Acknowledgements

References

[1] J.R. Wright, J.E. Cooper, Introduction to Aircraft Aeroelasticity and Loads, John Wiley & Sons, Ltd, 2007.

[2] D.J. Lucia, P.S. Beran, W.A. Silva, Reduced-order modeling: new approaches for computational physics, Prog. Aerosp. Sci. 40 (1–2) (2004) 51–117.

[3] P.S. Beran, D.J. Lucia, C.L. Pettit, Reduced-order modelling of limit-cycle oscillation for aeroelastic systems, J. Fluids Struct. 19 (2004) 575–590.

[4] T.J. Cowan, A.S. Arena, K.K. Gupta, Accelerating computational fluid dynamics based aeroelastic predictions using system identification, J. Aircr. 38 (1) (2001) 81–87.

[5] W.A. Silva, Recent Enhancements to the Development of CFD-Based Aeroelastic Reduced Order Models, AIAA Paper 2007-2051, 2007.

[6] W.A. Silva, Identification of nonlinear aeroelastic systems based on the Volterra theory: progress and opportunities, Nonlinear Dyn. 39 (1–2) (2005) 25–62.

[7] A. Mannarino, P. Mantegazza, Nonlinear aerodynamic reduced order modeling by discrete time recurrent neural networks, Aerosp. Sci. Technol. 47 (2015) 406–419.

[8] J.P. Thomas, E.H. Dowell, K.C. Hall, Three-dimensional transonic aeroelasticity using proper orthogonal decomposition-based reduced-order models, J. Aircr. 40 (3) (2003) 544–551.

[9] M. Dardel, F. Bakhtiari-Nejad, A reduced order of complete aeroelastic model for limit cycle oscillations, Aerosp. Sci. Technol. 14 (2) (2010) 95–105.

[10] Q. Zhou, G. Chen, A. Da Ronch, Y. Li, Reduced order unsteady aerodynamic model of a rigid aerofoil in gust encounters, Aerosp. Sci. Technol. 63 (2017) 203–213.

[11] B.P. Danowsky, P.M. Thompson, C. Farhat, T. Lieu, C. Harris, J. Lechniak, Incorporation of feedback control into a high-fidelity aeroservoelastic fighter aircraft model, J. Aircr. 47 (4) (2010) 1274–1282.

[12] A.R. Crowell, J.J. McNamara, K.M. Kecskemety, T.W. Goerig, A Reduced Order Aerothermodynamic Modeling Framework for Hypersonic Aerothermoelasticity, AIAA Paper 2010-2969, 2010.

[13] Q. Zhou, D. Li, A. Da Ronch, G. Chen, Y. Li, Computational fluid dynamics-based transonic flutter suppression with control delay, J. Fluids Struct. 66 (2016) 183–206.

[14] P. Marques, A. Da Ronch, Advanced UAV Aerodynamics, Flight Stability and Control: Novel Concepts, Theory and Applications, Wiley–Blackwell, 2017.

[15] S. Timme, K.J. Badcock, A. Da Ronch, Gust load analysis using computational fluid dynamics derived reduced order models, J. Fluids Struct. 71 (2017) 116–125.

[16] M. Ghoreyshi, R.M. Cummings, A. Da Ronch, K.J. Badcock, Transonic aerodynamic loads modeling of x-31 aircraft pitching motions, AIAA J. 51 (10) (2013) 2447–2464.

[17] C.L. Pettit, Uncertainty quantification in aeroelasticity: recent results and research challenges, J. Aircr. 41 (5) (2004) 1217–1229.

[18] Y. Dai, C. Yang, Methods and advances in the study of aeroelasticity with uncertainties, Chin. J. Aeronaut. 27 (3) (2014) 461–474.

[19] D.M. Pitt, D.P. Haudrich, M.J. Thomas, Probabilistic Aeroelastic Analysis and Its Implications on Flutter Margin Requirements, AIAA Paper 2008-2198, 2008.

[20] C. Scarth, J.E. Cooper, P.M. Weaver, G.H.C. Silva, Uncertainty quantification of aeroelastic stability of composite plate wings using lamination parameters, Compos. Struct. 116 (2014) 84–93.

[21] J. Deng, C. Anton, Y.S. Wong, Stochastic collocation method for secondary bifurcation of a nonlinear aeroelastic system, J. Sound Vib. 330 (13) (2011) 3006–3023.

[22] X. Wang, Z. Qiu, Interval finite element analysis of wing flutter, Chin. J. Aeronaut. 21 (2) (2008) 134–140.

[23] R.M. Lind, M. Brenner, Robust Aeroservoelastic Stability Analysis: Flight Test Applications, Springer-Verlag, 1999.

[24] H. Yun, J. Han, Robust flutter analysis of a nonlinear aeroelastic system with parametric uncertainties, Aerosp. Sci. Technol. 13 (2–3) (2009) 139–149.

[25] B. Moulin, M. Idan, M. Karpel, Aeroservoelastic structural and control optimization using robust design schemes, J. Guid. Control Dyn. 25 (1) (2002) 152–159.

[26] B.P. Danowsky, J.R. Chrstos, D.H. Klyde, C. Farhat, M. Brenner, Evaluation of aeroelastic uncertainty analysis methods, J. Aircr. 47 (4) (2010) 1266–1273.

[27] S. Heinze, D. Borglund, Robust flutter analysis considering mode shape variations, J. Aircr. 45 (3) (2008) 1070–1074.

[28] R. Lind, M. Brenner, Analyzing Aeroservoelastic Stability Margins Using the μ Method, AIAA Paper 1998-1895, 1998.

[29] B. Moulin, Modeling of aeroservoelastic systems with structural and aerodynamic variations, AIAA J. 43 (12) (2005) 2503–2513.

[30] C.L. Martin, K. Anders, Industrial application of robust aeroelastic analysis, J. Aircr. 48 (4) (2011) 1176–1183.

[31] Y. Gu, Z. Yang, Robust Flutter Analysis of an Airfoil with Flap Freeplay Uncertainty, AIAA Paper 2008-2201, 2008.

[32] M. Karpel, B. Moulin, M. Idan, Robust aeroservoelastic design with structural variations and modeling uncertainties, J. Aircr. 40 (5) (2003) 946–954.

[33] T. Lieu, C. Farhat, M. Lesoinne, Reduced-order fluid/structure modeling of a complete aircraft configuration, Comput. Methods Appl. Mech. Eng. 195 (41–43) (2006) 5730–5742.

[34] H. Liu, H. Hu, Y. Zhao, R. Huang, Efficient reduced-order modeling of unsteady aerodynamics robust to flight parameter variations, J. Fluids Struct. 49 (2014) 728–741.

[35] W. Zhang, K. Chen, Z. Ye, Unsteady aerodynamic reduced-order modeling of an aeroelastic wing using arbitrary mode shapes, J. Fluids Struct. 58 (2015) 254–270.

[36] J. Slotnick, A. Khodadoust, J. Alonso, D. Darmofal, W. Gropp, E. Lurie, D. Mavriplis, CFD Vision 2030 Study: A Path to Revolutionary Computational Aerosciences, NASA TR NASA/CR-2014-218178, NF1676L-18332, 2014.

[37] L. Eça, M. Hoekstra, A procedure for the estimation of the numerical uncertainty of CFD calculations based on grid refinement studies, J. Comput. Phys. 262 (2014) 104–130.

[38] T. Barth, On the propagation of statistical model parameter uncertainty in CFD calculations, Theor. Comput. Fluid Dyn. 26 (5) (2012) 435–457.

[39] Z. Qiu, P.C. Müller, A. Frommer, An approximate method for the standard interval eigenvalue problem of real non-symmetric interval matrices, Commun. Numer. Methods Eng. 17 (4) (2001) 239–251.

[40] L. Meirovitch, Computational Methods in Structural Dynamics, Sijthoff & Noordhoff, 1980.

[41] K. Isogai, On the transonic-dip mechanism of flutter of a sweptback wing, AIAA J. 17 (7) (1979) 793–795.

[42] K. Isogai, Transonic dip mechanism of flutter of a sweptback wing: part II, AIAA J. 19 (9) (1981) 1240–1242.

[43] X. Wang, L. Wang, Uncertainty quantification and propagation analysis of structures based on measurement data, Math. Comput. Model. 54 (11–12) (2011) 2725–2735.

[44] J.J. Alonso, A. Jameson, Fully-Implicit Time-Marching Aeroelastic Solutions, AIAA Paper 1994-0056, 1994.

[45] F. Liu, J. Cai, Y. Zhu, H.M. Tsai, A.S.F. Wong, Calculation of wing flutter by a coupled fluid–structure method, J. Aircr. 38 (2) (2001) 334–342.

[46] E.C. Yates Jr., N.S. Land, J.T. Foughner Jr., Measured and Calculated Subsonic and Transonic Flutter Characteristics of a 45° Swepteback Wing Planform in Air and in Freon-12 in the Langley Transonic Dynamics Tunnel, NASA TN D-1616, 1963.

[47] E.C. Yates Jr., AGARD Standard Aeroelastic Configurations for Dynamic Response I. – Wing 445.6, NASA TM 100492, 1987.

[48] E.M. Leerausch, J.T. Batina, Wing flutter boundary prediction using unsteady Euler aerodynamic method, J. Aircr. 32 (2) (1995) 416–422.